

“Atmospheric ammonia variability and link with PM formation: a case study over the Paris area” by Camille Viatte et al.

Anonymous Referee #1

Authors: We would like to thank the referee for his/her insightful comments. We have made changes to the manuscript to address those comments.

Referee: This manuscript uses observations from two independent satellites to assess the role of NH₃ in springtime particle pollution episodes in the Paris region by examining the seasonal and interannual variability (IAV) in NH₃ columns over northwestern Europe.

The observations are compared to simulations from the CHIMERE chemical transport model. In general, the authors do a good job of reviewing the existing literature to provide context for their results, but it would be useful if they could include a comparison with the study of Schiferl et al. (2016), which examines seasonal cycles and IAV of NH₃ over the US.

Authors: We have added sentences in the revised manuscript to compare with the interesting study of Schiferl et al., (2016):

In section 3.1.2: “In addition, inter-annual variabilities of NH₃ concentrations over the United-States are dominated by meteorological conditions [Schiferl et al., 2016].”

In section 3.2.1: “This is a different finding than in Schiferl et al. (2016) since they restricted IASI high relative errors when comparing to the GEOS-Chem model over the United-States, which inherently favors larger columns and thus lead to weaken the observed seasonal cycle.”

Referee: In Section 2.2, it is important that the authors report what proportion of the column observations from each satellite were below the limit of detection and how those data were incorporated into the monthly means used throughout the paper. If observations below the limit of detection were discarded, then the resulting monthly means will be biased high. It would then be important to filter the model output in a similar way to ensure that the observation-model comparison is more appropriate.

Authors: As mentioned in the manuscript, IASI’s detection limit is 4-6 10¹⁵ molecules/cm². Observations below this detection limits represent about 60% of the 2014-2015 dataset. Those were not discarded when computing monthly means. CrIS’s detection limit is 1-2 10¹⁵ molecules/cm² but no observations in the current product are reported (Shephard et al., 2019). This is a potential reason why CrIS is high compared to IASI in absolute values (See figure R1). However, when comparing to the model data, we

selected CHIMERE outputs located within the same 0.15°x0.15° grid box than the satellite and within 1 hour from its measurement to ensure that the comparisons are appropriate.

We now have added a sentence about this difference in averaging IASI and CrIS when comparing monthly means to the model outputs in section 3.2.1: “Note that values below detection limits have not been filtered out from the IASI dataset whereas the quality flag was used to discard CrIS’s retrievals associated with DOFS<=0.1 (Section 2.2.2) favors larger observed columns. Consequently, the normalized seasonal cycle amplitude derived from CrIS is weaker than the IASI one.”

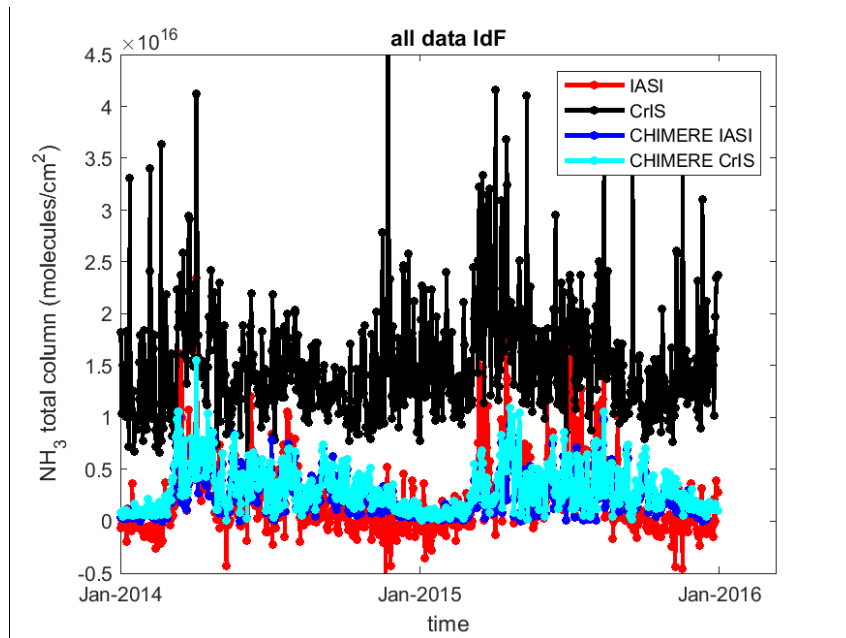


Figure R1: Time series of daily mean NH₃ concentrations (in molecules/cm²) derived from IASI and CrIS satellite measurements (red and black, respectively), and from the CHIMERE model outputs coincident in space and time with IASI (in blue) and CrIS (in cyan).

Referee: A general concern in Section 3.1 is the confidence with which the authors interpret the causes contributing to the seasonality and IAV of the ammonia columns. In many cases, the explanations provided by the authors seem reasonable, but unless there is conclusive proof, the language should be toned down to indicate that these are possible/likely explanations rather than the only ones:

Referee: Lines 282-301, a handful of data are provided to describe farming practices in different regions, but not in a consistent way. What evidence is there that the factors described are the most important in causing the spatial and temporal patterns observed?

Authors: We have changed the tone of the text, it is now: “The observed seasonality is mainly related to agricultural practices (fertilizer application period varying as function of the crop types and type of

livestock) and changes in temperatures, with higher temperatures favoring volatilization. This likely explains the high concentration in July and August.”

Referee: Lines 313-314 How do crop type and phenological stage impact ammonia concentrations leading to interannual variability?

Authors: The phenological stage controls the fertilizer spreading dates, driving NH_3 emissions, and consequently, is likely to regulate NH_3 Inter-annual variability observed in a specific region.

We have added details in the manuscript: “It has been recently shown that spatial variability of NH_3 emissions in France is due to fertilizer use and type and pedoclimatic conditions, and that temporal variability depends on seasonal timing of fertilizer applications [Ramanantenasoa et al., 2018]. In addition, inter-annual variabilities of NH_3 concentrations over the United-States are dominated by meteorological conditions [Schiferl et al., 2016]. Thus, inter-annual variability of observed NH_3 total columns is likely to be driven by meteorological conditions and specific agricultural constrains (crop type and phenological stage for instance).”

Referee: Lines 330-333 These seem like plausible explanation for the impact of precipitation amount of ammonia columns, but is there direct evidence that they are the only (most) important factors?

Authors: We added likely and toned down our language throughout this section and in the conclusion.

Referee: Lines 334-335 The relationship between gas phase ammonia and temperature should be exponential based on the temperature dependence of its volatilization (either vapor pressure or effective solubility). Does the correlation coefficient change if a non-linear fit is tried?

Authors: We have checked and found a correlation of $R = 0.30$ instead of 0.33 when using a linear fit. We have rectified the manuscript accordingly. The residuals of the fit, however are similar when trying linear and exponential based fitting.

Referee: In Section 3.2, the authors compare ‘standardized’ monthly means for the years 2014 and 2015 between the two satellite products and the model. More explanation should be provided about how these standardized means were calculated. Do the emissions used in the model differ between the two years? This would be useful to know to help in interpreting the variability produced by the model.

Authors: We have included the computation equations regarding the standardization in the 2.4 section: “The standardized columns have been computed following equation 1:

$$X_{stand}^{data} = \frac{(X^{data} - \mu(X^{data}))}{S(X^{data})} \quad (1)$$

Where $(X^{data}) = \frac{1}{N} \sum_{i=1}^N X_i^{data}$, $S(X^{data}) = \sqrt{\frac{1}{N-1} \sum_{i=1}^N (X_i - \mu)^2}$, X^{data} corresponds to NH₃ columns derived from a dataset (IASI, CrIS, or CHIMERE), and X_{stand}^{data} is the corresponding standardized dataset. ”

The emissions of the model are the same for the 2 years of simulations; the interannual variability of the model is therefore likely to be attributed to meteorological conditions changes. We have clarified in the text that the emissions were the same for the two years and have added a sentence: “In addition, year-to-year variability can be seen in the model with lower concentrations in March 2015 compared to 2014 for instance, despite constant emissions in the 2-years simulation. This interannual variability is likely to be attributed to meteorological conditions changes.”

Referee: Lines 371-382 This discussion is a bit confusing because initially the values quoted from the correlation plots of are the coefficients of determination, and then the comparison is restricted to select months and the values quoted are the slopes. I would recommend quoting the r² values for both, to make it more clear that the coefficients of determination did not increase significantly when the months were restricted. Also, the fact that the slope is close to 1 is not that meaningful since each dataset has already been standardized.

Authors: We have changed the text accordingly by removing the slope values and adding p-value instead:

“Over the whole period, the coefficient of determination (r²) between the standardized monthly mean NH₃ columns derived from IASI (CrIS), and the CHIMERE model is 0.58 (0.18) for the annual cycles of 2014 and 2015 with low associated p-values of 1.5 10⁻⁵ (0.06) reflecting the significance level of the fits (not shown here). If we only consider months of high NH₃ in the domain from March to August, the correlation between the observational datasets and the model is rather good with r² values between IASI (CrIS) and CHIMERE of 0.29 (0.14) with associated p-values of 0.07 (0.24), as shown in Figure 7. Since annual total emissions are the same for the two years and simply disaggregated with a monthly profile in the model, the correlations reveal that the seasonal cycle is likely to be reproduced by the model. In addition, year-to-year variability can be seen in the model with lower concentrations in March 2015 compared to 2014 for instance, despite constant emissions in the 2-years simulation. This interannual variability is likely to be attributed to meteorological conditions changes. However, the values of the r² lower than 0.5 indicate that the CHIMERE model only reproduces at most half of the observed monthly temporal NH₃ variabilities in the domain. Similar variabilities are found between the observations and the model outputs since the coefficients of correlation of the standard deviations are 0.4 and 0.6 between CHIMERE and IASI and CrIS, respectively.”

We have also changed the abstract accordingly:

“A detailed analysis of the seasonal cycle is performed using both IASI and the CrIS instrument data, together with outputs from the CHIMERE atmospheric model. For 2014 and 2015 the CHIMERE model shows coefficient of determination of 0.58 and 0.18 when comparing with IASI and CrIS, respectively.”

Referee: In Section 3.3, which focuses on the role of NH_3 in producing $\text{PM}_{2.5}$ in the Ile de France region, the analysis is overly simplistic. Why have the $\text{PM}_{2.5}$ observations included in the analysis been restricted the measurements between 9 and 11 am? This time interval is particularly challenging to interpret because of the impacts of primary emissions and the role of the rapidly changing boundary layer height. It seems like a poor choice of time window to focus on a phenomenon that is influenced by long-range/ regional transport of a precursor species like NH_3 . The role of temperature and relative humidity on the formation of ammonium salts is well-described by thermodynamic relationships. Statements like those on Lines 504-509 are not fully accurate.

Authors: Over the studied area, Metop-A and Metop-B have an overpass time difference ranging from only a few seconds to 67 minutes depending on the viewing geometry of the satellite scans; the average difference is of 26 minutes for the 1325 days of common measurements. Over the whole time period IASI (MetopA and B) overpass time is about 9.50am on average. Therefore we have selected $\text{PM}_{2.5}$ data between 9 and 11 am to study cases in which $\text{PM}_{2.5}$ and NH_3 (observations averaged with MetopA and B) concentrations are enhanced simultaneously (or within a one-hour interval) over the IdF region. We also tried a similar analysis considering $\text{PM}_{2.5}$ measured at 10am only and averaged all day (between 8am and 6pm), and this did not change our results regarding the number of events detected for case A and B.

Concerning the statements concerning the role of temperature and humidity on the formation of ammonium salts, we have added ‘mainly’ and ‘in particular’ to be more accurate: “Our observations are in agreement with previous studies [Bessagnet et al., 2016; Wang et al., 2015], which have shown that the formation of ammonium salt needs a specific humidity of 60 - 70%, mainly because it corresponds to the deliquescence point of NH_4NO_3 in ambient air. This is in agreement with our results since the mean of relative humidity in case A is 70%. Our results also support the idea that a relatively low atmospheric temperature favor $\text{PM}_{2.5}$ formation in particular since the phase equilibrium leads to NH_4NO_3 decomposition above 30 °C.”

Specific comments:

Referee: Line 46 – ‘biochemical’ should perhaps be ‘biogeochemical’

Authors: We changed this.

Referee: Line 63 – ‘related to’ should be ‘relative to’

Authors: We changed this.

Referee: Line 111-114 – It would be helpful to reword the sentence slightly, to clarify that all of the studies being referenced were carried out in Paris.

Authors: We have reworded this sentence as: “However, although the Paris megacity is repeatedly shrouded by particulate pollution episodes, many studies are limited in the Paris megacity and performed over relatively short time frame during field campaigns: NH₃ measurements from May 2010 to February 2011 [Petetin et al., 2016] and nitrate, sulfate, and ammonium aerosol measurements in July 2009 [Zhang et al., 2013], or based on numerical simulations [Skyllakou et al., 2014].”

Referee: Figure 1 – The coloring of the map by the emissions is not easy to see. The colors become a very different shade on the map than on the legend. Is it possible to use a map that doesn’t have a green background, or to make the emissions coloring more opaque?

Authors: We changed the background of the map and made the emissions coloring more opaque.

Referee: Figure 6 – would be helpful to have the same months identified on the axis for each year

Authors: We have edited the figure to have the same months for the 2 years.

References: Shephard, M. W., Damers, E., Kharol, S., and Cady-Pereira, K.: Ammonia measurements from space with the Cross-track Infrared Sounder (CrIS): characteristics and applications, in preparation for ACP, 2019

“Atmospheric ammonia variability and link with PM formation: a case study over the Paris area” by Camille Viatte et al.

Anonymous Referee #2

Referee: In this study, Viatte et al. use satellite observations (CrIS, IASI) to a) characterize the spatial and inter annual variability of ammonia column over Western Europe and its drivers and b) examine the connection between NH₃ and PM_{2.5} over Paris. The material presented is interesting and well suited for ACP. However, I have some significant concerns regarding the robustness of some of the conclusions and the lack of connection between a) and b). These need to be addressed before I publication can be considered.

Authors: We would like to thank the referee for his/her insightful comments. We have performed additional analyses and adapted the manuscript to fully address those comments.

General Comments

Referee: a) there are places when the authors make fairly definitive claims with insufficient support/references.

For instance Line 49: it is stated that N causes species/ecosystem extinction. A specific reference is needed.

Authors: We have added 2 references for this sentence: [Isbell et al., 2013; Hernandez et al., 2016]

Referee: Line 341 and discussion above. This discussion is too speculative and needs to be much better supported. Was more corn planted in 2011 than in 2012? Were planting dates shifted earlier in 2011 relative to 2012? This is critical since the authors then state that they have shown that meteorology and farming practices account for the interannual variability in NH₃ column.

Authors: We have toned down our language to indicate that these are possible/likely explanations rather than the only ones.

Referee: Line 374 It is stated that the correlation is “good” based on Fig. 7 ($r^2 < 0.3$). What is the p value, what is the uncertainty on the slopes given the large error bars shows in Fig. 7? In general, the authors need to be more quantitative when reporting statistics: always give p value for correlation (e.g., line 331 and 333) and uncertainty for slopes.

Authors: We have changed “good” to “rather good”. As proposed by the other referee, the values of the slopes are not that meaningful since each dataset has already been standardized. Therefore we have removed the slope values and added the p-values for each r^2 values, as you suggested.

“Over the whole period, the coefficient of determination (r^2) between the standardized monthly mean NH_3 columns derived from IASI (CrIS), and the CHIMERE model is 0.58 (0.18) for the annual cycles of 2014 and 2015 with low associated p-values of $1.5 \cdot 10^{-5}$ (0.06) reflecting the significance level of the fits (not shown here). If we only consider months of high NH_3 in the domain from March to August, the correlation between the observational datasets and the model is rather good with r^2 values between IASI (CrIS) and CHIMERE of 0.29 (0.14) with associated p-values of 0.07 (0.24), as shown in Figure 7. Since annual total emissions are the same for the two years and simply disaggregated with a monthly profile in the model, the correlations reveal that the seasonal cycle is likely to be reproduced by the model. In addition, year-to-year variability can be seen in the model with lower concentrations in March 2015 compared to 2014 for instance, despite constant emissions in the 2-years simulation. This interannual variability is likely to be attributed to meteorological conditions changes. However, the values of the r^2 lower than 0.5 indicate that the CHIMERE model only reproduces at most half of the observed monthly temporal NH_3 variabilities in the domain. Similar variabilities are found between the observations and the model outputs since the coefficients of correlation of the standard deviations are 0.4 and 0.6 between CHIMERE and IASI and CrIS, respectively.”

We have also changed the abstract accordingly:

“A detailed analysis of the seasonal cycle is performed using both IASI and the CrIS instrument data, together with outputs from the CHIMERE atmospheric model. For 2014 and 2015 the CHIMERE model shows coefficient of determination of 0.58 and 0.18 when comparing with IASI and CrIS, respectively.”

Referee: b) there is very little connection between a) and b) in the current manuscript. In part b), the authors focus on the relationship between $\text{PM}_{2.5}$ and NH_3 in two (fairly similar) years (2014, 2015). The main conclusion is that meteorology (temperature, local PBL) probably controls whether NH_3 contributes to $\text{PM}_{2.5}$. This is interesting although very much expected from studies performed in other regions. From part a), I was instead expecting the authors to consider whether the considerable variability in NH_3 sources over Belgium/Netherlands could impact $\text{PM}_{2.5}$ over Paris. From part a), I was also expecting to have the authors show whether CHIMERE is able to capture the observed correlation between $\text{PM}_{2.5}$ and NH_3 . This could help understand whether the observed $\text{PM}_{2.5}$ enhancement results from production of ammonium nitrate in Ile de France or from transport of ammonium nitrate/sulfate or other aerosols from Belgium. I fully appreciate that such analysis will require significant work. However, without a significantly stronger connection between part a) and b), I would recommend the paper be split, with part a) being more readily publishable.

Authors: We have added a section (3.3) and a Figure (new Figure 11) to evaluate the capacity of the model to reproduce $\text{PM}_{2.5}$ over the Parisian region.

“Comparisons of PM_{2.5} concentrations in IdF derived from the Airparif network and CHIMERE for 2014 and 2015

To evaluate the model capacity to reproduce PM_{2.5} concentrations over the Parisian region, comparisons between the Airparif measurements network and the CHIMERE outputs have been performed for 2014 and 2015 (Figure 11). For those years, concentrations of PM_{2.5} are measured hourly from the surface at 13 Airparif stations distributed over the IdF region (black dots, Figure 1). To compare with the CHIMERE model, we have extracted the hourly surface PM_{2.5} outputs in the IdF region, i. e. within a 50 km-radius circle from Paris.

Results of the comparison are shown in Figure 11. Day-to-Day variability of PM_{2.5} concentrations at the surface is well represented by the CHIMERE model with however differences during pollution events in March/April and in December for both years. The model may underestimate PM_{2.5} concentrations in spring due to unknown PM_{2.5} formation processes, but overestimate them in winter which could be due to uncertainties on NH₃ emissions from wood burning processes. Overall, good agreement is found between the measurements and the model in term of PM_{2.5} concentrations over the IdF region given values of r^2 of 0.56 (associated with p-value of $6 \cdot 10^{-133}$), a slope of 0.67 ± 3.51 , with a slightly underestimation of the CHIMERE model given a mean relative difference (calculated as model-observations/observations) of -18% over 2014 and 2015.”

We have also added a sentence in the conclusion about this analysis: “In this region, we also found that the CHIMERE model is able to reproduce the day-to-day variability of PM_{2.5} concentrations (r^2 of 0.56), with however an underestimation during spring pollution events, which could be due to unknown secondary aerosol formation processes.”

Finally, we have added a sentence in the abstract section about PM_{2.5} concentrations evaluation from CHIMERE: “In addition, PM_{2.5} concentrations derived from the CHIMERE model have been evaluated against surface measurements from the Airparif network over Paris. Agreement was found (r^2 of 0.56) with however an underestimation during spring pollution events.”

To investigate whether the variability in NH₃ sources over the northeast part of the domain could impact NH₃ over Paris, we have studied the cross-correlation function of NH₃ concentrations between the Northeast part of the domain (over the Netherlands) and the IdF region (see Figure R1 and Figure S5 in the supplement information). The cross-correlation function (CCF) is calculated between the daily averaged mean of the IASI NH₃ columns observed over these two regions (both are average values of available pixels of the same day). From the CCF plot, we can see that when lag = 0 (i.e. within the same day), the cross-correlation is maximum with CCF = 0.37, and the CCF is above 0.3 when lag=±1 (i.e. 1 day before or after) for the whole time period (2008-2016). Therefore, correlation between NH₃ concentrations over the northeast part of the domain and the IdF region is relatively correlated. This confirms the result suggested by the back-trajectory analysis in Figure 10. We have also computed the CCF over these two regions considering months with high NH₃: the maximum CCF between March and August and between March and April are 0.35 and 0.26, respectively. Therefore we have added a sentence about this analysis in the new section 3.4: “Indeed, NH₃ columns over the Netherlands are relatively correlated to NH₃ columns measured over IdF since the cross-correlation function is 0.37 at lag

= 0 and above 0.3 at lag = ± 1 day over the whole time period (2008-2016 - Figure S5).“ and we add a sentence in the abstract : “Variability of NH_3 in the Northeast region is likely to impact NH_3 concentrations in the Parisian region since the cross-correlation function is above 0.3 (at lag = 0 and 1). ”

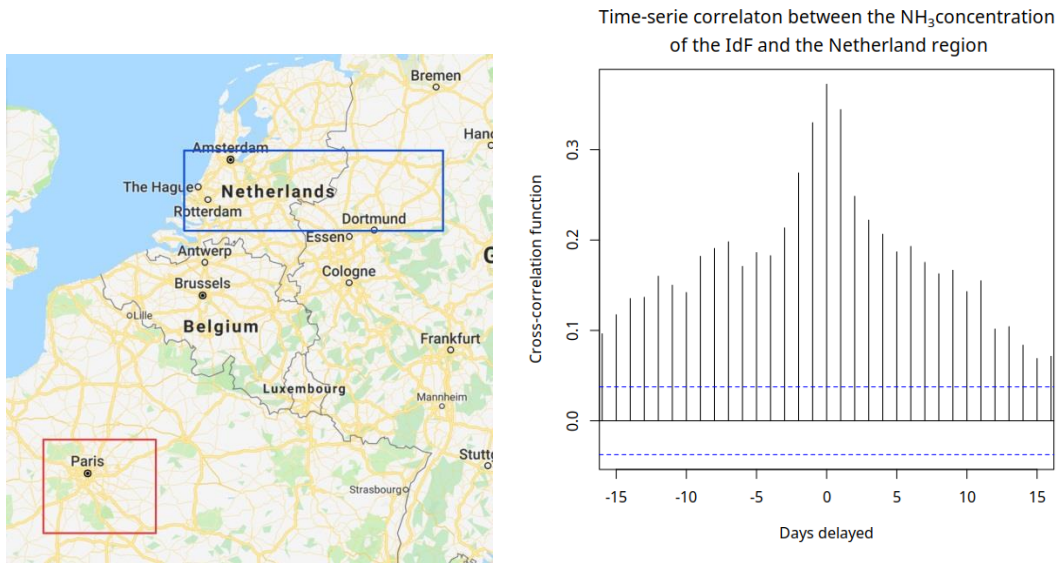


Figure R1: Cross-correlation analysis of NH_3 concentrations between the Northeast part of the domain (over the Netherlands) and the IdF region.

In addition, to study the effect of transport on NH_3 and $\text{PM}_{2.5}$ concentrations observed over the Parisian region, we have included wind fields analysis in Section 3.4 (old Section 3.3). In Figure 12 (old Figure 11) in the lower panel, we have added wind fields parameters (direction and speed) from ERA-5 and included wind roses for studies cases (ensemble, case A, and case B) in the supplement information. Results of the statistic show that cases involving simultaneous enhancements of NH_3 and $\text{PM}_{2.5}$ concentrations in Paris (cases A) are associated with wind fields dominantly coming from the Northeast. Air masses coming from this area are thus likely to favor simultaneous enhancements of NH_3 and $\text{PM}_{2.5}$ over Paris. We have added few sentences in the new Section 3.4 and the conclusion about this: Section 3.4: “Results also suggest that simultaneous enhancements of NH_3 and $\text{PM}_{2.5}$ over Paris (cases A) are mainly associated with wind fields dominantly coming from the Northeast part of the domain (Figure S6). Thus the combination of the following four meteorological parameters favors simultaneous appearances of NH_3 and of $\text{PM}_{2.5}$ in Paris (i.e. case A): low surface temperatures (5°C), with thin boundary layers ($\sim 500\text{m}$), rare precipitations, and northeast wind.” In the conclusion section: “To assess the link between NH_3 and $\text{PM}_{2.5}$ over the Parisian (IdF) region, the main meteorological parameters driving the optimal conditions involved in the $\text{PM}_{2.5}$ formation have been identified. The results show that relatively low temperature, thin boundary layer, coupled with almost no precipitation and wind coming from the northeast, favor the $\text{PM}_{2.5}$ formation with the presence of atmospheric NH_3 in the IdF region.”

Technical comments

Referee: Section 2.3 the description of CHIMERE is far too short (especially with respect to the treatment of ammonia. For instance: -> how is dry deposition represented? Does it include the bidirectional exchange between land and atmosphere -> what is the temporal resolution of the emissions? Does it include a diurnal cycle? It would be useful to show the seasonality of the emissions in a few regions, to help the reader better analyze Figs 2 and 3 -> how is the gas/aerosol partitioning of NH₃ represented (ISORROPIA?) -> I assume that NH₃/NH₄/NH₄NO₃ in CHIMERE have been evaluated previously? Please provide reference for these studies at this stage. I also encourage the authors to show how the configuration of CHIMERE that is used here performs against surface observations (e.g., EMEP wet deposition/concentrations). This could be briefly discussed in the main text, with figures in the supplementary materials.

Authors: We have detailed the description of the model by adding this section:

“These annual emissions are then distributed in hourly data to feed CHIMERE using seasonal, weekly and hourly factors. Fire emissions come from the Global Fire Assimilation System (GFAS, [Kaiser et al., 2012]).

The model computes hourly concentrations for more than 180 species, among which are the regulated pollutants such as ozone, PM₁₀, and NH₃. The processes that will influence the NH₃ concentrations taken into consideration in CHIMERE are the dry deposition (following [Wesely et al., 1989] and wet deposition due to in-cloud process and precipitations. The gas-particulate phase equilibrium is computed with the ISOROPPIA module [Nenes et al, 1998] which is a thermodynamic equilibrium model for NH₄⁺, NO₃⁻ and SO₄²⁻. It evaluates the NH₄NO₃ contribution to the particulate matter which is especially large during March-April pollution episodes [Petit et al., 2017].”

Referee: Section 3.1.1 It would be useful to include a map showing the distribution of livestock and major crops in Western Europe so that the reader can see the relationship between NH₃ emissions and the different sources described by the authors. This would be especially helpful as some of the material the authors refer to is in French.

Authors: We have added specific references for livestock mapping and found English versions of the references:

- <https://agriculture.gouv.fr/overview-french-agricultural-diversity> ;
- Scarlat et al., 2018 – their figure 2],
- [Robinson et al., 2014 - their figure 2c].

Referee: Fig. 5. This figures shows first and foremost that there is good correlation between skin temperature and precipitation at the regional level. I think it would be more relevant to show the relationship between temperature/precipitation and NH₃ anomaly. In addition, I assume that the precipitation/temperature anomalies exhibit some significant spatial variability? Do you weigh the anomaly by the average NH₃ column? High NH₃ columns only cover a small fraction of your domain and it's unclear to me why it would respond to the average temperature change (vs the local change).

Authors: We have tried the analysis suggested by the referee. Anomalies of NH₃ and temperature/precipitation over the domain are shown in Figure R2. The results suggests strong relationships exists between anomalies of NH₃ and skin temperature (correlation R = 0.72), and total precipitation (anti-correlation R = -52).

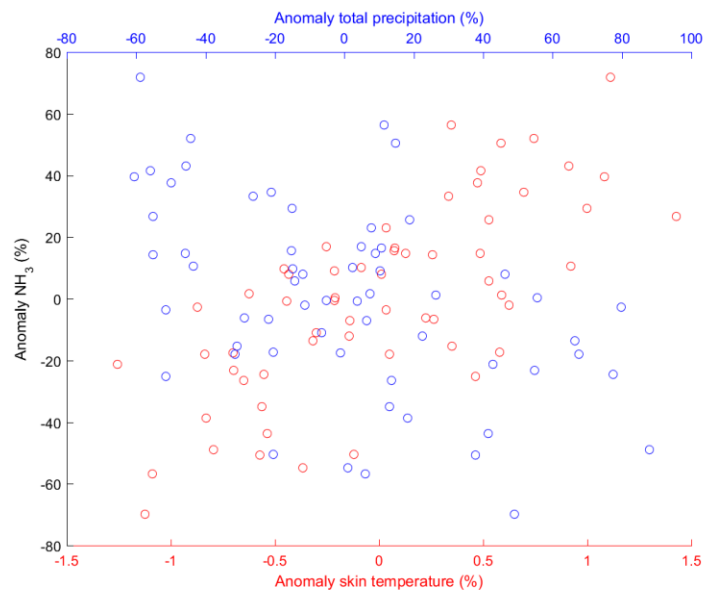


Figure R2: monthly mean anomaly (relative to the 10-years – 2008 to 2017 - monthly average) of total precipitation/skin temperature derived from ECMWF from March to August in the domain, versus NH₃ total columns anomaly derived from IASI.

When computing the anomalies, temperature and precipitation anomalies were not weighting by NH₃ total column.

Referee: Section 3.2. I am a little confused by the need for the standardization. CrIS and IASI seem reasonably close, so why not use the model absolute NH₃ column. In addition, Fig. 6 only show one CHIMERE time series, shouldn't there be two, one for CHIMERE sampled at the IASI overpass time and one at the CrIS overpass time (with AK)..

Authors: The CrIS and the IASI data are not close in absolute values: CrIS is higher than IASI in the region of interest (of about 1.10^{16} molecule/cm²). In addition, the CHIMERE output concentrations are closer to

IASI observations than CrIS's ones (see Figure R3), which is why we wanted to standardized each dataset independently. We have also tested the comparison between CrIS and CHIMERE by taking into account the different vertical sensitivity (smoothing by the AK) but results were not improved.

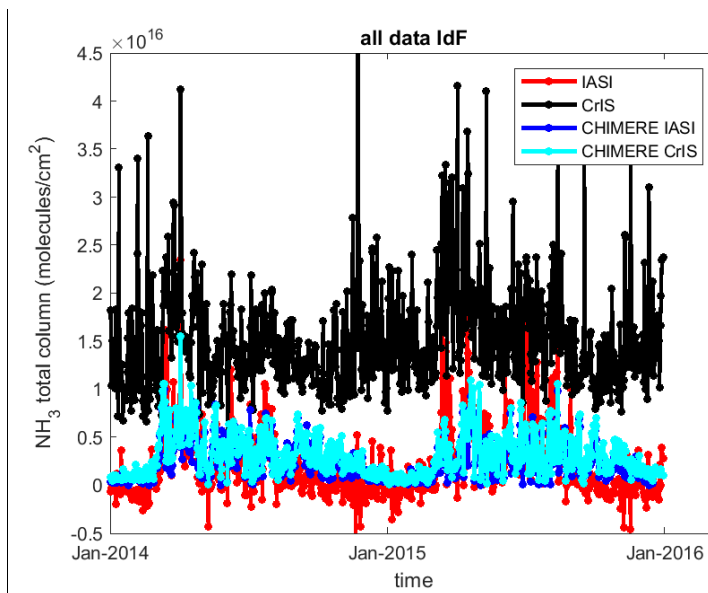


Figure R3: Time series of daily mean NH_3 concentrations (in molecules/cm²) derived from IASI and CrIS satellite measurements (red and black, respectively), and from the CHIMERE model outputs coincident in space and time with IASI (in blue) and CrIS (in cyan).

As for Figure 6, we have changed it to include the CHIMERE time series sampled in space and time with IASI and CrIS, as you suggested.

Referee: Line 351 I am not sure I understand the motivation for picking this years. Why not use the climatological seasonality? Why are these years more useful to benchmark the model? They look fairly similar as far as I can tell from the supporting material.

Authors: In the frame of evaluating the model capacity of reproducing NH_3 variability in space and time at regional scale and its impact on air quality at local scale, those two years are interesting for the following reasons.

At regional scale (over the 400 km radius around Paris), NH_3 total columns derived from IASI in 2014 and 2015 are highly variable in time throughout the years and especially in spring, reaching 10% higher in March and 50% lower in May than the 10-years average. Since ammonia emission variability depends on seasonal timing of fertilizer applications in France [Ramanantenasoa et al., 2018], this period is crucial to assess the model capacity.

Second, for those two years NH_3 concentrations over the IdF region (100 km radius around Paris) are also extremely high in March (Figure R4, upper panel). These extreme events might have affected the Parisian

air quality since $PM_{2.5}$ concentrations are also enhanced, especially in 2014 (Figure R4, lower panel). We have added this Figure in the Supplementary Information (Figure S1).

Therefore, we think these years could serve as benchmark to evaluate the model in terms of NH_3 variability at regional scale, and $PM_{2.5}$ formation at local scale. We have changed the manuscript to explain the motivation for choosing these years in section 2.3 dedicated to the CHIMERE model: “To evaluate the model capacity of reproducing NH_3 variability in space and time at regional scale and its impact on air quality at local scale, comparisons have been performed in 2014 and 2015 for the following reasons. At regional scale (over the 400 km radius around Paris), NH_3 total columns derived from IASI in 2014 and 2015 are highly variable in spring, reaching 10% higher in March and 50% lower in May than the 10-years average. Since ammonia emission variability in France depends on seasonal timing of fertilizer applications [Ramanantenasoa et al., 2018], this period is crucial to assess the model capacity. Second, the IdF region (100 km radius around Paris) also experiences high NH_3 and $PM_{2.5}$ events in spring 2014 and 2015 (Figure S1). Thus, these years serve as benchmark to evaluate the model in terms of NH_3 variability and $PM_{2.5}$ formation at local and regional scales.”

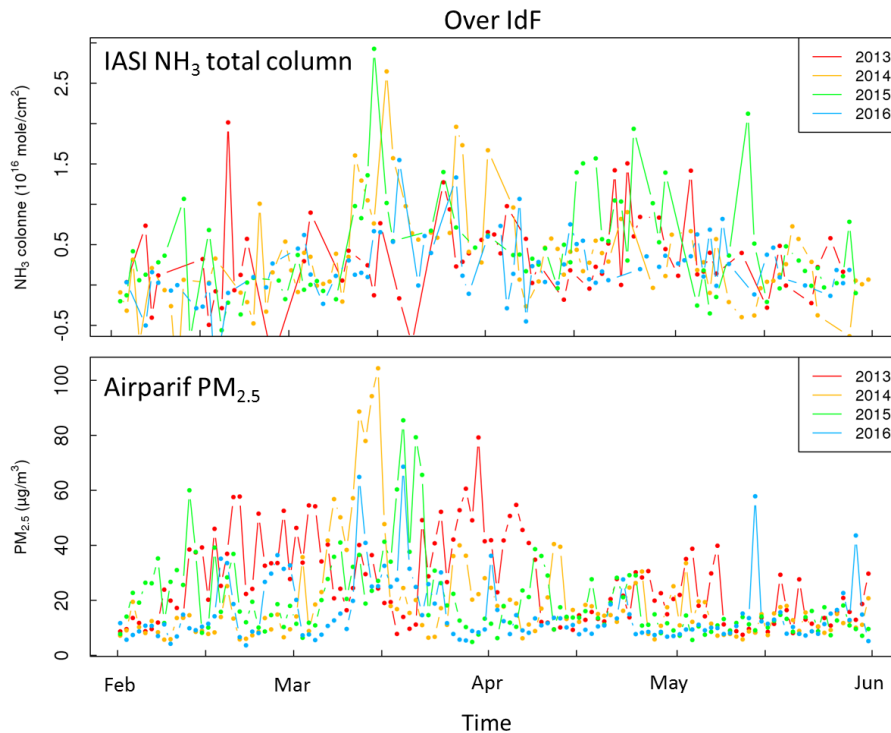


Figure R4: Time series of daily mean NH_3 concentrations (in molecules/cm²) derived from IASI (upper panel) and $PM_{2.5}$ concentration (in $\mu g/m^3$) observed over the IdF region between 2013 and 2016.

Technical comments

Referee: They are a few issues with language. It sometimes (rarely) makes it challenging to understand the manuscript.

Referee: line 28: regression slope. Remove slope

Authors: We have removed slope

Referee: line 63: related->relative

Authors: We have changed this.

Referee: Line 112: many of studies?

Authors: We have deleted "of"

Referee: Line 283: farming species? Do you mean livestock?

Authors: Yes, we have changed it to livestock.

Referee: Line 300. What are non-poultry granivorous (animals)?

Authors: We have deleted granivorous.

Referee: Fig. 7 What do the error bars correspond to?

Authors: The error bars correspond to the 1-sigma standard deviation around the mean. We have clarified it in the figure caption.

Referee: Fig. 9: Same than Fig.7 -> "Same as Fig. 8"

Authors: We have changed this.

Referee: Fig. 12: Define IQR

Authors: We added: The IQR is the "interquartile range", and it equals to $Q3 - Q1$ where $Q3$ and $Q1$ are the 75th and 25th percentiles. Setting the thresholds at $Q1 - 1.5 * IQR$ and $Q3 + 1.5 * IQR$ is a common practice to determine outliers.

Referee: Line 220: I don't understand the distinction between inorganic, organic and natural aerosols?

Authors: We have deleted this part of the text to include more specific description of the model.

Referee: Line 487. Why is the value given on line 476 different (mean/median?)

Authors: The first value refers to the example given in the manuscript, i. e. from March 3rd and March 19th 2014, whereas the second value represents the mean value for the case A over the whole dataset. We have added 'over the whole dataset' in the latest sentence to avoid confusion.

1 Atmospheric ammonia variability and link with PM formation: a
2 case study over the Paris area

3 Viatte Camille¹, Wang Tianze¹, Van Damme Martin², Dammers Enrico³, Meleux Frederik⁴,
4 Clarisse Lieven², Shephard Mark W.³, Whitburn Simon², Coheur Pierre François², Cady-Pereira
5 Karen E.⁵, and Clerbaux Cathy^{1,2}

6 ¹ LATMOS/IPSL, Sorbonne Université, UVSQ, CNRS, Paris, France

7 ² Université libre de Bruxelles (ULB), Service de Chimie Quantique et Photophysique, Atmospheric
8 Spectroscopy, Brussels, Belgium

9 ³ Environment and Climate Change Canada, Toronto, Ontario, Canada

10 ⁴ Institut national de l'environnement industriel et des risques, INERIS, Verneuil en Halatte, France

11 ⁵ Atmospheric and Environmental Research (AER), Inc., Lexington, USA

12 Abstract

13 The Paris megacity experiences frequent particulate matter (PM_{2.5}, PM with a diameter less than
14 2.5 μm) pollution episodes in springtime (March-April). At this time of the year, large parts of
15 the particles consist of ammonium sulfate and nitrate which are formed from ammonia (NH₃)
16 released during fertilizer spreading practices and transported from the surrounding areas to
17 Paris. There is still limited knowledge on the emission sources around Paris, their magnitude and
18 seasonality.

19 Using space-borne NH₃ observation records of 10-years (2008-2017) and 5-years (2013-2017)
20 provided by the Infrared Atmospheric Sounding Interferometer (IASI) and the Cross-Track
21 Infrared Sounder (CrIS) instrument, regional pattern of NH₃ variabilities (seasonal and inter-
22 annual) are derived. Observations reveal identical high seasonal variabilities with three major
23 NH₃ hot spots found from March to August. The high inter-annual variability is discussed with
24 respect to atmospheric total precipitation and temperature.

25 A detailed analysis of the seasonal cycle is performed using both IASI and the CrIS instrument
26 data, together with outputs from the CHIMERE atmospheric model. For 2014 and 2015 the
27 CHIMERE model shows coefficient of determination of 0.58 and 0.18 when comparing with IASI
28 and CrIS, respectively. A detailed analysis of the seasonal cycle is performed using both IASI and
29 the CrIS instrument data, together with outputs from the CHIMERE atmospheric model. For
30 months of high NH₃ concentrations (March to August) the CHIMERE model shows good
31 correspondence with correlation slopes of 0.98 and 0.71 when comparing with IASI and CrIS,
32 respectively. It is found that the model is only able to reproduce half of the observed
33 atmospheric temporal NH₃ variability in the domain. In term of spatial variability, the CHIMERE
34 monthly NH₃ concentrations in springtime show a slight underrepresentation over Belgium and
35 the United-Kingdom and overrepresentation in agricultural areas in the French Brittany/Pays de
36 la Loire and Plateau du Jura region, as well as in the north part of Switzerland. In addition, PM_{2.5}
37 concentrations derived from the CHIMERE model have been evaluated against surface
38 measurements from the Airparif network over Paris. Agreement was found (r² of 0.56) with
39 however an underestimation during spring pollution events.

40 Using HYSPLIT cluster analysis of back-trajectories, we show that NH₃ total columns measured in
41 spring over Paris are enhanced when air masses are originated from the Northeast (e. g.,
42 Netherlands and Belgium), highlighting the long-range transport importance on the NH₃ budget
43 over Paris. Variability of NH₃ in the Northeast region is likely to impact NH₃ concentrations in the
44 Parisian region since the cross-correlation function is above 0.3 (at lag = 0 and 1).

45 Finally, we quantify the key meteorological parameters driving the specific conditions important
46 for the PM_{2.5} formation from NH₃ in the Ile-de-France region in springtime. Data-driven results

47 based on surface PM_{2.5} measurements from the Airparif network and IASI NH₃ observations
48 show that a combination of the factors, e. g. a low boundary layer of ~500m, a relatively low
49 | temperature of 5°C, ~~and~~ a high relative humidity of 70%, and wind from the Northeast
50 contributes to favor PM_{2.5} and NH₃ correlation.

51 1. Introduction

52 Ammonia (NH₃) is an atmospheric pollutant and one of the main sources of reactive nitrogen in
53 the atmosphere which is involved in numerous ~~biochemical~~biogeochemical exchanges
54 impacting all ecosystems [Sutton et al., 2013]. The global budget of reactive N has dramatically
55 increased since the preindustrial era [Holland et al., 2005; Battye et al., 2017] causing major
56 environmental damages such as ecosystems and species extinction [Isbell et al., 2013;
57 Hernandez et al., 2016], as well as soil and water eutrophication and acidification [Rockström et
58 al., 2009]. NH₃ is a precursor of ammonium salts which can form up to 50% to particulate matter
59 (PM) total mass [Behera et al., 2013]. Large cities such as Paris (which is the most populated
60 area in the European Union with 10.5 million people when its larger metropolitan regions are
61 included) typically experiences strong PM pollution episodes in springtime. These particles are
62 known to be harmful for human health [Pope III et al., 2009] inducing 2000 deaths per year in
63 the Paris megacity [Corso et al., 2016] and to impact the radiative budget of the Earth [Myhre et
64 al., 2013].

65 Because of their impact on the environment, public health, and climate change, NH₃ emissions
66 are regulated in several countries in the world. However, NH₃ emissions of European countries
67 have increased by 2% over the period 2014-2016 [National Emission Ceilings Directive reporting
68 status, 2018], where the Gothenburg Protocol set a reduction of 6% by 2020. In France, where
69 94% of NH₃ emissions come from the agriculture sector [CITEPA, 2018] as a result of extensive
70 fertilizer use to increase crop yields [Erisman et al., 2008], policies have been implemented with
71 the aim to reduce NH₃ emissions by 13% in 2030 ~~relative~~iveed to 2005 [CEIP, 2016]. However NH₃
72 emissions are projected to increase in the future globally with increased population and food
73 demand [van Vuuren et al., 2011] and NH₃ volatilization will be enhanced with climate change
74 [Sutton et al., 2013].

75 Once in the atmosphere, NH₃ is rapidly removed by wet and dry deposition, and by reactions
76 with atmospheric sulfuric and nitric acid, leading to a relatively short lifetime between a few
77 hours and few days [Galloway et al., 2003]. Release of NH₃ in the atmosphere depends on i)
78 agriculture practices: spreading season, fertilizer form (urea, ammonium nitrate), fertilizer
79 application methods, crops, soil conditions such as pH [Hamaoui-Laguel et al., 2014]; and on ii)
80 meteorological conditions (i.e. wind, temperature, and precipitation). Inter-annual variability of
81 PM formation over urban area is poorly understood, since it also depends on many factors such
82 as atmospheric humidity and temperature, which govern the phase equilibrium of secondary
83 aerosols [Fuzzi et al., 2015]. The variety of factors influencing NH₃ volatilization and PM
84 formation illustrates the complexity of predicting their concentrations in the atmosphere
85 [Behera et al., 2013].

86 Atmospheric chemical transport models have difficulty representing both NH_3 and $\text{PM}_{2.5}$
87 distributions due to the challenge of reproducing NH_3 temporal variability [Pinder et al., 2006;
88 Fortems-Cheiney et al., 2016], long-range transport of pollutants [Moran et al., 2014], and
89 secondary aerosol formation in the atmosphere [Petetin et al., 2016]. The GEOS-Chem chemical
90 transport model [Bey et al., 2001] was found to underestimate the observed NH_3 concentrations
91 in most regions of the globe [Zhu et al., 2013; Li et al., 2017]. Heald et al. (2012) compared the
92 IASI observations with the GEOS-Chem model and showed that NH_3 is likely underestimated in
93 California, leading to a local underestimate of ammonium nitrate aerosol. Similarly, the French
94 CHIMERE model [Menut et al., 2013] underestimates the NH_3 budget over Paris [Petetin et al.,
95 2016; Fortems-Cheiney et al., 2016] because of the mis-representation of agricultural emissions
96 in terms of intensity and both spatial and temporal distribution. Often ground and aircraft-
97 based observations are used to provide detailed representation of the atmospheric state that
98 can be used to evaluate and improve the model simulations; however, these can be spatially
99 sparse and/or over short sampling periods, especially globally. Additionally, more recently
100 available (within the last 10-years) sun-synchronous satellite-based infrared sensors have been
101 providing NH_3 observations globally with a spatial resolution of ~ 15 km approximately twice a
102 day. These satellite observations have limited independent vertical information, but do capture
103 the spatiotemporal variabilities needed to help address these issues and improve model
104 simulations, especially in remote locations [Skjøth et al., 2011; Kranenburg et al., 2016].

105 Aside from the Tropospheric Emission Spectrometer (TES, [Beer et al., 2008]), now
106 decommissioned but which was first to demonstrate the capability of thermal infrared
107 instruments to monitoring lower tropospheric NH_3 , 3 missions are able to measure it now : the
108 Atmospheric InfraRed Sounder (AIRS, [Warner et al., 2016]), the Cross-track Infrared Sounder
109 (CrIS, [Shephard and Cady-Pereira, 2015]), and the Infrared Atmospheric Sounding
110 Interferometer (IASI, [Clarisse et al., 2009]). Recent studies have shown the increased capacity
111 of space-borne instruments to derived spatial and seasonal distributions of NH_3 concentrations
112 globally [Clarisse et al., 2009; Shephard et al., 2011; Van Damme et al., 2014a & 2015a],
113 regionally [Beer et al., 2008; Clarisse et al., 2010; Van Damme et al., 2014b] and locally [Van
114 Damme et al., 2018], as well as trends of NH_3 [Warner et al., 2017].

115 Representative measurements of NH_3 concentrations and spatiotemporal variabilities are
116 needed to address the link between NH_3 and $\text{PM}_{2.5}$ formation and improve model simulations.
117 This has been attempted previously in some cities around the world, such as in Shanghai [Ye et
118 al., 2011], Houston [Gong et al., 2013], Santiago City [Toro et al., 2014], and Beijing [Zhao et al.,
119 2016] for instance. However, although the Paris megacity is repeatedly shrouded by particulate
120 pollution episodes, many ~~of~~ studies are limited in the Paris megacity and performed over
121 relatively short time frame during field campaigns: NH_3 measurements from -May 2010 to
122 February 2011 [Petetin et al., 2016] and nitrate, sulfate, and ammonium aerosol measurements

123 | [in July 2009](#); [Zhang et al., 2013], or based on numerical simulations [Skylakou et al., 2014]. Our
124 study is a data-driven regional approach and considers a longer time period to study the
125 seasonal/inter-annual variabilities of NH_3 and its impact of $\text{PM}_{2.5}$ formation over the Paris
126 megacity. Specifically in this paper we study concentrations and spatiotemporal variability of
127 atmospheric NH_3 from the agricultural sector to gain insights on its effects on megacity air
128 quality using: 1) long-term satellite observations derived from IASI (10 years from 2008 to 2017)
129 and CrIS (5 years from 2013 to 2017) at regional scale (400km radius-circle from Paris city
130 center); 2) spatiotemporal patterns of the CHIMERE model evaluated against the IASI and CrIS
131 datasets for 2014 and 2015; and 3) the main meteorological parameters favoring the secondary
132 $\text{PM}_{2.5}$ formation from NH_3 in the Paris megacity are analyzed.

133 2. Methodology

134 2.1. Region of analysis

135 The domain of analysis covers a circular area of 400 km radius around the Paris city center
136 (Figure 1, larger circle) enabling the study of temporal and spatial variabilities of NH_3 emission
137 sources likely to affect air quality in the Paris megacity. It has been selected for two reasons.
138 First, it includes main regions known for their high NH_3 emissions, which can be transported and
139 affect air quality over the Parisian region (Ile-de-France -IdF-, smaller circle in Figure 1).
140 Emission regions in the Netherlands, North of Germany, Northwest of Belgium, and the Brittany
141 region in France, are highlighted in darker colors in Figure 1 (emissions values are from the
142 European Monitoring and Evaluation Programme -EMEP- 2015). Second, this area corresponds
143 to the transport of 24 hours back-trajectories from Paris generated from the HYSPLIT model for
144 one year, ensuring that NH_3 can indeed be efficiently transported from the emitting sources
145 within the selected domain to the IdF region.

146 2.2. Satellite observations of ammonia

147 For this study we used the available data from IASI and CrIS which are both Fourier transform
148 spectrometers to evaluate the current capacity to observe NH_3 concentrations from space, and
149 study its variability around IdF. Technical information are summarized in Table 1.

150 2.2.1. Infrared Atmospheric Sounding Interferometer (IASI)

151 IASI is a nadir-viewing spectrometer launched on board the Metop-A and Metop-B satellites and
152 operated by EUMETSAT (European Organisation for the Exploitation of Meteorological
153 Satellites), since October 2006 and September 2012, respectively. These satellites are on similar
154 polar orbits with Equator crossing times at 09:30 (21:30) local mean solar time for the
155 descending (ascending) orbit. IASI measures the thermal infrared radiation of the system Earth-
156 atmosphere in the spectral range from 645 to 2760 cm^{-1} with a spectral resolution 0.5 cm^{-1}

157 apodized. The satellite swath is an area of 2200 km width composed by off-nadir measurements
158 up to 48.3° on both sides of the track. At nadir, the IASI field of view is composed of 4 x 4 pixels
159 of 12 km diameter each [Clerbaux et al., 2009].

160 The NH_3 total columns used here are derived from IASI using an Artificial Neural Network
161 reanalyzed with ERA-interim data (ANNI-NH3-v2.1R [Van Damme et al., 2017]). This dataset is
162 consistent in time and suitable for investigating inter-annual variability, which is one purpose of
163 this study. Note that we have considered here only morning measurements (9:30) since the
164 evening ones (21:30) are associated with larger relative errors [Van Damme et al., 2017]. IASI
165 retrievals provide a robust error estimate for each IASI-NH3 observations, allowing to take into
166 account the variable sensitivity when comparing IASI dataset with independent measurements.
167 Finally, no filter on relative errors of the IASI datasets has been applied following
168 recommendations from Van Damme et al. (2017) and outliers for which concentrations exceed
169 10 standard deviations above the mean in the domain of study have been removed.

170 Over the studied area, Metop-A and Metop-B have an overpass time difference ranging from
171 only a few seconds to 67 minutes depending on the viewing geometry of the satellite scans; the
172 average difference is 26 minutes for the 1325 days of common measurements. Monthly maps
173 for the 10 years of observations between 2008 and 2017 are obtained by averaging Metop-A
174 and whenever Metop-B (the two instruments are considered jointly for their period of common
175 operation from March 2013 to 2017) with more than 10^5 pixels on average over the domain of
176 analysis. The number of available NH_3 columns depends not only on the satellite overpass time
177 but also on the state of the atmosphere being remotely sensed (e.g. thermal contrast and cloud
178 cover). IASI NH_3 has been evaluated using the LOTOS-EUROS model over Europe [Van Damme et
179 al., 2014b] and ground-based and airborne measurements [Van Damme et al., 2015b], showing
180 consistency between the IASI NH_3 and the available datasets. When comparing IASI NH_3
181 (previous IASI-NN version) with ground-based Fourier transform infrared (FTIR) observations, a
182 correlation of 0.8 and a slope of 0.73, with a mean relative difference of $-32.4 \pm (56.3)\%$ have
183 been found [Dammers et al., 2016].

184 2.2.2. Cross-track Infrared Sounder (CrIS)

185 The CrIS instrument [Zavalyov et al., 2013] is a Fourier Transform spectrometer operated by the
186 Joint Polar Satellite System (JPSS) program on Suomi National Polar-orbiting Partnership (NPP)
187 satellite, launched on 28 October 2011. CrIS is in a sun-synchronous orbit with a mean local
188 daytime overpass time of 13:30 (01:30) in the ascending (descending) node. CrIS measures the
189 atmospheric composition over three wavelength bands in the infrared region ($645\text{--}1095\text{ cm}^{-1}$;
190 $1210\text{--}1750\text{ cm}^{-1}$; $2155\text{--}2550\text{ cm}^{-1}$). NH_3 retrievals are performed from the $645\text{--}1095\text{ cm}^{-1}$ band
191 with a spectral resolution of 0.625 cm^{-1} . The CrIS instrument scans a 2200 km swath width (+/-

192 50 °). At nadir, the CrIS field of view consists of a 3 × 3 array of circular pixels of 14 km diameter
193 each.

194 The CrIS Fast Physical Retrieval (CRPR) [Shephard and Cady-Pereira., 2015] uses an optimal
195 estimation approach [Rodgers, 2000] that minimizes the difference between the CrIS measured
196 atmospheric spectra and a very fast Optimal Spectral Sampling (OSS) [Moncet et al., 2008]
197 forward model simulated spectrum to retrieve atmospheric profiles of ammonia volume mixing
198 ratios. This physical approach provides direct estimates of the retrieval errors and the vertical
199 sensitivity (averaging kernels) of the satellite observations, which is important as they vary from
200 profile-to-profile depending on the atmospheric state. The retrieved error covariance and
201 averaging kernels are also beneficial for air quality model comparisons and data assimilation
202 into models as any *a priori* information used in the retrieval can be accounted for in a robust
203 manner (i.e. observation operator). CrIS has been shown to retrieve ammonia surface
204 concentrations values down to ~0.2-0.3 ppbv under favorable conditions [Kharol, et al., 2018].
205 CrIS comparisons with ground-based FTIR observations show a correlation of 0.77 with a low
206 CrIS bias of +2% in the total column [Dammers et al., 2017]. Initial evaluation against surface
207 observations from the Ammonia Monitoring Network (AMoN) show that even with the inherent
208 sampling differences between the two surface observations they compare well with a
209 correlation of 0.76 and an overall mean CrIS – AMoN difference of ~+15% [Kharol et al., 2018].

210 For this study, the CrIS quality flag = 4 has been used, ensuring that retrievals provide some
211 information from the measurement (degrees-of-freedom- of-signal $\text{DOFS} > 0.1$). In addition,
212 outliers for which concentrations exceed 10 standard deviations above the mean have been
213 removed.

214 2.3. Modelling NH₃ from the CHIMERE model

215 The CHIMERE runs used in this study were obtained in the framework of the Copernicus
216 Atmospheric Monitoring Service (CAMS, <https://atmosphere.copernicus.eu/>), and its annual
217 task devoted to the production of regional reanalysis over Europe. The hindcasts for year 2014
218 and 2015 (raw simulation without data assimilation) were produced over Europe with a
219 horizontal resolution of 0.1° per 0.1° and
220 9 vertical levels stretched from the surface up to 500 hPa (~5000m). The input data to feed
221 CHIMERE [Menut et al., 2013; Mailler et al., 2017] were the Integrated Forecasting System (IFS)
222 meteorological data from European Centre for Medium-Range Weather Forecasts (ECMWF), the
223 annual emission inventory provided by the Netherlands Organisation for Applied Scientific
224 Research (TNO) [Kuenen et al., 2014] for year 2011. These annual emissions are then distributed
225 in hourly data to feed CHIMERE using seasonal, weekly and hourly factors. Fire emissions come
226 from the Global Fire Assimilation System (GFAS, [Kaiser et al., 2012]).

227 ~~and the fire emissions from the Global Fire Assimilation System (GFAS, [Kaiser et al., 2012]).~~The
228 model computes hourly concentrations for more than 180 species, among which are the
229 regulated pollutants such as ozone, PM₁₀, and NH₃. The processes that will influence the NH₃
230 concentrations taken into consideration in CHIMERE are the dry deposition (following [Wesely
231 et al., 1989] and wet deposition due to in-cloud process and precipitations. The gas-particulate
232 phase equilibrium is computed with the ISOROPPIA module [Nenes et al, 1998] which is a
233 thermodynamic equilibrium model for NH₄⁺, NO₃⁻ and SO₄²⁻. It evaluates the NH₄NO₃
234 contribution to the particulate matter which is especially large during March-April pollution
235 episodes [Petit et al., 2017].

236 ~~Within CHIMERE a comprehensive modelling system allows to compute the evolutions of~~
237 ~~gaseous species and aerosols taking into account physical and chemical process. More than 30~~
238 ~~gaseous species are involved in the chemical scheme and an aerosol module assesses the gas-~~
239 ~~particulate phase equilibrium and compute the aerosol composition (inorganic, organic and~~
240 ~~natural components). These datasets were evaluated over Europe for several pollutants before~~
241 ~~being used for air quality studies (<http://policy.atmosphere.copernicus.eu/Reports.html>).~~

242 The model NH₃ profiles were integrated vertically along the 9 km model layers to provide a
243 column that can be compared to that of the satellite measurements. Concretely this makes the
244 reasonable assumption that all the NH₃ is located within this 0-5km layer (see e.g. Figure 1 in
245 [Whitburn et al., 2016]).

246 To evaluate the model capacity of reproducing NH₃ variability in space and time at regional scale
247 and its impact on air quality at local scale, comparisons have been performed in 2014 and 2015
248 for - the following different reasons. At regional scale (over the 400 km radius around Paris), NH₃
249 total columns derived from IASI in 2014 and 2015 are highly variable in spring, reaching 10%
250 higher in March and 50% lower in May than the 10-years average. Since ammonia emission
251 variability in France depends on seasonal timing of fertilizer applications [Ramanantenasoa et
252 al., 2018], this period is crucial to assess the model capacity. Second, the IdF region (100 km
253 radius around Paris) also experiences high NH₃ and PM_{2.5} events in spring 2014 and 2015 (Figure
254 S1). Thus, these years serve as benchmark to evaluate the model in terms of NH₃ variability and
255 PM_{2.5} formation at local and regional scales.

256 2.4. Relative scales and coincidence criteria for dataset comparisons

257 Direct quantitative comparisons of satellite NH₃ products are difficult because of the different
258 overpass times and ground footprint sizes of the 2 space borne instruments, which are not
259 compatible with the high variability of NH₃ in space and time. Therefore, the evaluation of
260 satellite observations is often made with the use of in situ measurements performed at surface

261 and onboard aircrafts [Nowak et al., 2012; Van Damme et al., 2015b], or with ground-based
262 remote-sounding FTIR [Dammers et al., 2016; Dammers et al., 2017].

263 The purpose here of comparing CrIS and IASI is to assess qualitatively the spatiotemporal
264 patterns of the NH₃ sources derived from the two datasets and use these regional observations
265 to evaluate the CHIMERE model in the domain of analysis at the local time for their respective
266 overpasses: 9:30 and 13:30. CHIMERE outputs, in terms of NH₃ concentrations, have already
267 been compared to the IASI observations at regional scale (Europe, [Fortems-Cheiney et al.,
268 2016]), and to surface measurements at local scale (Paris, [Petetin et al., 2016]), but have never
269 been evaluated against the CrIS observations.

270 One aspect that needs to be considered when comparing concentration amounts inferred from
271 infrared satellite observations is the importance of the algorithm and the a priori information
272 used in the retrieval, especially for NH₃ which has limited vertical information. Some differences
273 between the IASI and CrIS observations might arise due to instrument measurement differences
274 (e.g. sensitivity), difference sampling period (e.g. overpass times of morning/evening vs middle
275 of day/night), and retrieval algorithm differences, but they have both been validated and shown
276 to capture well the spatiotemporal variations in lower tropospheric ammonia. Since the purpose
277 of our study is not to quantitatively compare IASI and CrIS NH₃ data, but rather to use these
278 independent datasets to assess NH₃ sources patterns over the domain and qualitatively
279 evaluate the CHIMERE model in term of NH₃ concentrations and variabilities, a standardization
280 procedure was applied to their retrieved absolute NH₃ columns. We computed “standardized
281 columns” for each independent dataset (IASI, CrIS, and CHIMERE, separately) for 2014 and 2015
282 over the domain of study in such a way that the corresponding values have a standard deviation
283 of 1 and a mean of 0, as in [Wilks, 2011].

284 The standardized columns have been computed following equation 1:

285
$$X_{stand}^{data} = \frac{(X^{data} - \mu(X^{data}))}{S(X^{data})} \quad (1)$$

286 Where $(X^{data}) = \frac{1}{N} \sum_{i=1}^N X_i^{data}$, $S(X^{data}) = \sqrt{\frac{1}{N-1} \sum_{i=1}^N (X_i - \mu)^2}$, X^{data} corresponds to NH₃
287 columns derived from a dataset (IASI, CrIS, or CHIMERE), and X_{stand}^{data} is the corresponding
288 standardized dataset.

289 In addition, to compare CHIMERE outputs with satellite data/columns, spatial and temporal
290 coincidence criteria have been applied. To compare satellite observations, all CrIS pixels located
291 within a 25-km radius circle from the center of the IASI ground pixels have been considered
292 within the same day of measurements. A spatial criterion of 25 km has been chosen because it
293 optimizes the number of pairs involved in the statistics and improves the correlations. As for the

294 comparisons between the model and the observations: all CHIMERE outputs located within the
295 same 0.15°x0.15° grid box than the satellite and within 1 hour from its measurement have been
296 selected.

297 3. Results

298 3.1. NH₃ regional observations derived from IASI (10-years) and CrIS (5- 299 years)

300 3.1.1. Seasonal variabilities

301 First the seasonal variability was investigated over the IdF area. On a monthly basis, the 10-year
302 and 5-year averaged regional NH₃ total column distributions derived from IASI and CrIS were
303 found to exhibit a high seasonality over the domain (Figures 2 and 3). Note that the distributions
304 in Figures 2 and 3 have been obtained by averaging satellite NH₃ observations in 0.25°x 0.25°
305 grid boxes. Both satellite datasets exhibits the same variability over the domain even if the time
306 period is different (10-years versus 5-years) and the sampling hour differs (~9.30 versus ~13.30).
307 One note that CrIS and IASI NH₃ columns present small differences in term of NH₃ total columns
308 in low concentration regimes in the domain of study.

309 In these figures (2 and 3) high NH₃ concentrations (up to 2.10¹⁶ molecules/cm²) can be observed
310 from March to August at different locations of the domain:

- 311 • The French Champagne-Ardennes region in March and April (Figures 2 and 3, box A),
- 312 • The northern part of the domain corresponding to the Netherlands and the North of Belgium
313 from April to August (Figures 2 and 3, box B), and
- 314 • The Brittany/Pays de la Loire regions (West of France) mainly in April and August but still
315 persistent from March to August (Figures 2 and 3, box C).

316 The observed seasonality is mainly related to agricultural practices (fertilizer application period
317 varying as function of the crop types and type of farming species/livestock) and changes in
318 temperatures, with higher temperatures favoring volatilization. This likely explains the high
319 concentration in July and August.

320 In the Champagne-Ardennes region, areas of hotspots do not correspond to vineyards but to
321 field vegetables and root crops ([https://agriculture.gouv.fr/overview-french-agricultural-](https://agriculture.gouv.fr/overview-french-agricultural-diversityfrom-the-Institut-National-de-la-Recherche-Agronomique-INRA)
322 [diversityfrom the Institut National de la Recherche Agronomique INRA](https://odr.inra.fr/intranet/carto/cartowiki/index.php/OTEX_et_Orientation_Agricole_des_terri)
323 https://odr.inra.fr/intranet/carto/cartowiki/index.php/OTEX_et_Orientation_Agricole_des_terri
324 [toires](http://agreste.agriculture.gouv.fr/IMG/pdf/R4215A15.pdf), and AGRESTE, Service Central d'Enquêtes et d'Études Statistiques, 2015
325 <http://agreste.agriculture.gouv.fr/IMG/pdf/R4215A15.pdf>). This is a leader region for mineral
326 fertilization used for sugar industry in France [Ramanantenasoa et al., 2018]. Hamaoui-Laguel et
327 al. (2014) and Fortems-Cheiney et al. (2016) have previously noted that NH₃ emissions in this

328 region, mainly due to fertilizer over barley, sugar beet, and potato starch in early March, were
329 higher than what have been reported in the EMEP inventory.

330 NH₃ concentrations are high from April to August in the northern part of the domain that is
331 known for its animal farming (Eurostat 2014, [http://ec.europa.eu/eurostat/statistics-
332 explained/index.php?title=File:Livestock_density_by_NUTS_2_regions,_EU-28,_2013.png](http://ec.europa.eu/eurostat/statistics-explained/index.php?title=File:Livestock_density_by_NUTS_2_regions,_EU-28,_2013.png), [Van
333 Damme et al., 2014a; [Scarlat et al., 2018 – their figure 2](#)]).

334 In the Pays de la Loire, NH₃ concentrations are high in April and August and remain relatively
335 high from March to September. Hotspots are found in areas of livestock farming, mainly poultry
336 ~~and granivorous~~ [\[Robinson et al., 2014 - their figure 2c\]](#), which ~~might~~ explains the high and
337 relatively constant NH₃ concentrations over warmer periods in this region.

338 3.1.2. Inter-annual variabilities

339 As can be seen in Figures 2 and 3, NH₃ concentrations are enhanced between March and August
340 in the domain. In this section, inter-annual variabilities are discussed regarding meteorological
341 conditions and agricultural practices during this time period.

342 Inter-annual variability of NH₃ is higher in springtime than in summer, e.g. in June the variance is
343 8 times lower than for the other months. To illustrate the inter-annual variability in springtime,
344 maps of monthly mean NH₃ total columns derived in March-April period from IASI (2008-2017
345 time period) and from CrIS (2013-2017 time period) are shown in Figure 4. Both satellite
346 distributions exhibit the same inter-annual variability from 2013 to 2017 with higher NH₃
347 concentrations in 2015 over the northern part of the domain than the other years. NH₃
348 concentrations derived from IASI in 2011 are 150% higher in spring (March and April) compared
349 to 2016 (Figure 4). [It has been recently shown that spatial variability of NH₃ emissions in France
350 is due to fertilizer use and type and pedoclimatic conditions, and that temporal variability
351 depends on seasonal timing of fertilizer applications \[Ramanantenasoa et al., 2018\]. In addition,
352 inter-annual variabilities of NH₃ concentrations over the United-States are dominated by
353 meteorological conditions \[Schiferl et al., 2016\]. Thus, ~~is-~~inter-annual variability of observed NH₃
354 total columns is likely to be partly driven by meteorological conditions and specific agricultural
355 constrains \(crop type and phenological stage for instance\).](#)

356 To investigate the impact of meteorological conditions on atmospheric NH₃ variability, we
357 computed the monthly mean anomalies of total precipitation versus skin temperature derived
358 from ECMWF ERA-interim [Dee et al., 2011], color coded by NH₃ total columns anomalies
359 derived from IASI, as shown in Figure 5. Monthly mean anomalies have been calculated relative
360 to the 10-years averages (in %). In this figure, monthly NH₃ total columns are at least 10% higher
361 (positive anomalies, red dots) when skin temperatures are higher and total precipitation are
362 lower than the 10-year average. In contrast, negative monthly NH₃ total columns anomalies

363 (blue dots, Figure 5) are associated with higher total precipitation and lower skin temperatures
364 than the 10-years average. To further detail this analysis, Figure 1 of the supplement
365 information shows bar plots of monthly mean NH₃ total columns derived from IASI, total
366 precipitation and skin temperature derived from ECMWF from March to August, plotted in
367 different colors for the different years of measurements from 2008 to 2017. NH₃ total columns
368 are larger by more than 300% in March-April 2012 compared to 2013 (Figure S24a). Total
369 precipitation is higher (0.4 mm compared to 1 mm, Figure S24b) and skin temperature is lower
370 (281 compared to 288 K, Figure S24c) in March 2013 than in March 2012 on average over the
371 domain. Overall, total precipitation is anti-correlated with NH₃ concentrations in the
372 atmosphere (R = -0.52 from March to MayAugust for all years, not shown here) likely because of
373 a) the wet deposition importance in the atmospheric NH₃ removal and b) the absence of
374 fertilization during rainy periods. Skin temperature is relatively correlated with NH₃
375 concentrations (R = 0.303 from March to MayAugust for all years) since higher temperature
376 increases volatilization of NH₃ from the surface to the atmosphere.

377 In addition, NH₃ concentration is maximum in March 2011 whereas it peaks later in April for
378 2012 (Figure S24a). Springtime is a spreading fertilizer period depending on many agricultural
379 and meteorological constrains. When temperature are mild, such as in 2012 (Figure S24b),
380 fertilizer spreading may occurs sooner because the phenological growth stage might be is more
381 advanced. Fertilizing process period also varies in function of the sowing date which depends on
382 agricultural practices and crop types: corn is fertilized in early spring whereas rapeseed is in late
383 spring.

384 Overall, all these meteorological (precipitation and temperature) and agricultural (fertilizer and
385 manure applications) parameters are possible factors to account for the high NH₃ inter-annual
386 variabilities revealed by both IASI and CrIS in the domain of study.

387 3.2. Comparisons of NH₃ columns derived from IASI, CrIS, and CHIMERE 388 for 2014 and 2015

389 To discuss the representation of agricultural emissions in the models in terms of intensity and
390 both spatial and temporal distributions, regional satellite observations derived from IASI and
391 CrIS have been compared to the CHIMERE model in the region of analysis.

392 3.2.1. Annual cycle

393 Standardized monthly mean concentrations derived from IASI, CrIS, and CHIMERE for 2014 and
394 2015 are shown in Figure 6. ~~These years were selected as NH₃ total columns were found to vary~~
395 ~~a lot, reaching 10% higher in March and 50% lower in May than the 10 years average.~~

396 As can be seen from the plot, the 3 datasets exhibit similar patterns in terms of seasonality: all
397 are enhanced in March-April and in summer, and show a decrease in May. However two major
398 differences can be noted.

399 First, CrIS standardized NH₃ columns are higher in winter (November, December, and January)
400 compared to the other dataset which can be also be seen in Figure 3. This could be attributed to
401 a higher number of outliers, given the larger standard deviation (shaded areas, Figure 6) and no
402 attempt to account for potential non-detects when concentrations fall below the instrument
403 detection limits. For these months, NH₃ levels are low and undetectable by satellite
404 observations (Figures 2 and 3) so these high values could be interpreted as observational noise.
405 The detection limit depends on the instrument characteristics and atmospheric state, with IASI
406 minimum detection limit of ~2-3 ppbv (~4-6.10¹⁵ molecules.cm⁻²) [Clarisse et al., 2010] and CrIS
407 ~0.5-1.0 ppbv (~1-2.10¹⁵ molecules.cm⁻²) [Shephard and Cady-Pereira, 2015; Kharol et. al.,
408 2018]. Note that values below detection limits have not been filtered out from the IASI dataset
409 whereas the quality flag was used to discard CrIS's retrievals associated with DOFS<=0.1
410 (Section 2.2.2) favors larger observed columns. Consequently, the normalized seasonal cycle
411 amplitude derived from CrIS is weaker than the IASI one.

412 Second, the CHIMERE standardized NH₃ columns are enhanced in September 2014, which is not
413 supported by the observations. It has been recently shown that CHIMERE overestimated NH₃
414 emissions in autumn over Europe [Couvidat et al., 2018]. Generally, the amplitude of the
415 modelled seasonal cycle exceeds the measured ones, which could be explained by higher
416 concentrations measured in winter due to the observational noise and lower emissions. This is a
417 different finding than in Schiferl et al. (2016) since they restricted IASI high relative errors when
418 comparing to the GEOS-Chem model over the United-States, which inherently favors larger
419 columns and thus lead to weaken the observed seasonal cycle.

420 Over the whole period, the coefficient of determination (r^2) between the standardized monthly
421 mean NH₃ columns derived from IASI (CrIS), and the CHIMERE model is 0.58 (0.18) for the
422 annual cycles of 2014 and 2015 with low associated p-values of 1.5 10⁻⁵ (0.06) reflecting the
423 significance level of the fits (not shown here). If we only consider months of high NH₃ in the
424 domain from March to August, the correlation between the observational datasets and the
425 model is rather good with r² values linear regression slope values between IASI (CrIS) and
426 CHIMERE of 0.290.98 (0.1474) with associated p-values of 0.07 (0.24), as shown in Figure 7.
427 Since annual total emissions are the same for the two years and simply disaggregated with a
428 monthly profile in the model, the correlations reveal that the seasonal cycle is likely to be
429 reproduced by the model. In addition, year-to-year variability can be seen in the model with
430 lower concentrations in March 2015 compared to 2014 for instance, despite constant emissions
431 in the 2-years simulation. This interannual variability is likely to be attributed to meteorological

432 | conditions changes. However, the values of the r^2 lower than 0.5 indicate that the CHIMERE
433 model only reproduces at most half of the observed monthly temporal NH_3 variabilities in the
434 domain. Similar variabilities are found between the observations and the model outputs since
435 the coefficients of correlation of the standard deviations are 0.4 and 0.6 between CHIMERE and
436 IASI and CrIS, respectively.

437 3.2.2. Spatial variability of NH_3 in springtime

438 The IASI and CrIS regional maps have been compared to the CHIMERE model for the March-April
439 period in 2014 and 2015 to evaluate the model's capacity to reproduce the spatial distribution
440 of the episodic emissions from fertilizer spreading practices in springtime, as well as their inter-
441 annual variability. Satellite NH_3 measurements in springtime have been gridded at $0.15^\circ \times 0.15^\circ$
442 spatial resolution, and the associated CHIMERE maps have been computed following the
443 coincident criteria described in section 2.4 at the same spatial resolution (Figures 8 and 9).

444 First one can notice that the spatial distribution of NH_3 observed in springtime by both satellite
445 instruments are in good agreement, even though their overpass time is different (~4 hours
446 apart). This was already seen in the inter-annual variability agreement seen in Figure 4. In spring
447 2014, IASI and CrIS both reveal three main regions of enhanced NH_3 concentrations (North,
448 Champagne-Ardennes, and Brittany/Pays de la Loire region) already identified by the 10-years
449 and 5-years of IASI and CrIS observation maps (Boxes A, B, and C of Figures 2 and 3). In 2015,
450 concentrations of NH_3 in the northern part of the domain are higher than in 2014, as indicated
451 by both IASI and CrIS observations (Figure 9, upper panels). Overall, satellite observations are
452 able to capture similar spatial distributions of high NH_3 concentrations in springtime, and their
453 evolution in time.

454 In spring 2014, the CHIMERE model reproduces the high concentrations in the three regions of
455 the domain identified in Figures 2 and 3. Additional NH_3 hot spots in the southeastern part of
456 the domain including the Po Valley, Switzerland, and the wine region between Besancon and
457 Lyon (blue box in Figure 8) are indicated by the CHIMERE model. NH_3 emissions in this latter
458 region are comparable to average agricultural plains over France. Only dispersion conditions
459 related to wind speed and boundary layer height can explain high NH_3 concentrations over this
460 area.

461 In spring 2015, satellite observations and the CHIMERE model outputs exhibit very similar
462 patterns in term of high NH_3 distributions, with however higher NH_3 concentrations indicated by
463 the model in the southern part of the domain (blue box in Figure 9).

464 Finally, the (model - observations) differences between the standardized NH_3 column derived
465 from the satellite instruments in springtime 2014-2015 and the corresponding NH_3 columns
466 derived from the CHIMERE model are shown in Figure 2 of the supplement information. One

467 can see that very similar patterns are presented when comparing the model to independent
468 satellite observations from IASI and CrIS: the modelled NH_3 concentrations are systematically
469 lower for both years over Belgium and United Kingdom, and higher in the southern part of the
470 domain (green square, Figure S32) including the Pays de la Loire region (box C in Figures 2 and
471 3), and in the southeastern part of the domain (over the North part of Switzerland and the
472 Plateau du Jura region - between Besancon and Lyon cities – blue box in Figure 8). Reasons of
473 enhanced NH_3 columns derived from the model in this latter region are not clear yet. An
474 explanation could be that the temporal distribution of the emissions is misrepresented in the
475 model since the modelled concentrations are enhanced in April whereas the two satellite
476 observations are enhanced earlier in March for both years. It is worth noting that there are no
477 EMEP stations measuring surface NH_3 concentrations in these regions. As for the Brittany/Pays
478 de la Loire region, it has already been shown that the LOTOS-EUROS atmospheric model [Schaap
479 et al., 2008] using similar chemistry schemes and NH_3 emissions shows higher columns each
480 year in this area [Van Damme et al., 2014b].

481 3.3. Comparisons of $\text{PM}_{2.5}$ concentrations in IdF derived from the Airparif 482 network and CHIMERE for 2014 and 2015

483 To evaluate the model capacity to reproduce $\text{PM}_{2.5}$ concentrations over the Parisian region,
484 comparisons between the Airparif measurements network and the CHIMERE outputs have been
485 performed for 2014 and 2015 (Figure 11). For those years, concentrations of $\text{PM}_{2.5}$ are
486 measured hourly from the surface at 13 Airparif stations distributed over the IdF region (black
487 dots, Figure 1). To compare with the CHIMERE model, we have extracted the hourly surface
488 $\text{PM}_{2.5}$ outputs in the IdF region, i. e. within a 50 km-radius circle from Paris.

489 Results of the comparison are shown in Figure 11. Day-to-Day variability of $\text{PM}_{2.5}$ concentrations
490 at the surface is well represented by the CHIMERE model with however differences during
491 pollution events in March/April and in December for both years. The model may underestimate
492 $\text{PM}_{2.5}$ concentrations in spring due to unknown $\text{PM}_{2.5}$ formation processes, but overestimate
493 them in winter which could be due to uncertainties on NH_3 emissions from wood burning
494 processes. Overall, good agreement is found between the measurements and the model in term
495 of $\text{PM}_{2.5}$ concentrations over the IdF region given values of r^2 of 0.56 (associated with p-value of
496 $6 \cdot 10^{-133}$), a slope of 0.67 ± 3.51 , with a slightly underestimation of the CHIMERE model given a
497 mean relative difference (calculated as model-observations/observations) of
498 -18% over 2014 and 2015.

499 3.3. Conditions for PM formation in the Paris megacity

500 3.4. Conditions for PM formation in the Paris megacity

501 To investigate the impact of intensive agriculture practices on the Paris megacity air quality, we
502 need to better understand the role of NH_3 in the formation of $\text{PM}_{2.5}$ that depends, among
503 others, on specific meteorological conditions such as atmospheric temperature and humidity
504 that alter the gas-particle partitioning. The link between high NH_3 concentrations inducing $\text{PM}_{2.5}$
505 formation in the Paris megacity is known [Petetin et al., 2016; Zhang et al., 2013] but
506 quantification of such phenomena is difficult due the lack of long-term NH_3 monitoring in the
507 IdF region. $\text{PM}_{2.5}$ is however measured hourly at several locations in Paris by the Airparif
508 network (<https://www.airparif.asso.fr/>, Figure 1). Thanks to the 10 years of IASI observations,
509 an observational evidence of $\text{PM}_{2.5}$ formation in the IdF region (100 km around Paris - black box
510 in Figure 1) is represented in Figure S43. Simultaneous enhancements in March of $\text{PM}_{2.5}$
511 measured at the surface and NH_3 columns derived from the IASI observations over the IdF
512 region are clearly visible. However, high concentrations of NH_3 observed in summer are not
513 associated with high $\text{PM}_{2.5}$ concentrations. This reflects the complexity of the $\text{PM}_{2.5}$ formation
514 depending on various factors, such as NH_3 emissions, atmospheric chemistry (acidic content of
515 the atmosphere), transport, and specific meteorological conditions involved in the gas to solid
516 phase conversion between NH_3 and ammonium salts.

517 To evaluate the impact of long-range transport on NH_3 levels observed over the Parisian region
518 (IdF) in spring, back-trajectory analysis was performed. In total 231 24-hours back-trajectories
519 ending in Paris (period from February 15th to May 15th from 2013 to 2016) were classified into 8
520 clusters using HYSPLIT (<https://ready.arl.noaa.gov/HYSPLIT.php>). Figure 10 shows the mean
521 trajectories for each cluster associated with the average NH_3 total columns measured by IASI
522 over the IdF region. In this figure, higher NH_3 columns are found under the influence of air
523 masses transported from the northern part of the domain (over Belgium and the Netherlands,
524 clusters 4 and 5) and from the Brittany region (cluster 8), which are the major sources regions of
525 NH_3 in spring in the domain as previously identified (Figures 2 and 3). Indeed, NH_3 columns over
526 the Netherlands are relatively correlated to NH_3 columns measured over IdF since the cross-
527 correlation function is 0.37 at lag = 0 and above 0.3 at lag = ± 1 day over the whole time period
528 (2008-2016 - Figure S5). Clusters 2 and 3 (Figure 10) are associated with intermediate NH_3 levels
529 since air masses moved slowly transporting NH_3 -rich air from rural regions near IdF (such as the
530 Champagne-Ardennes region - Box A in Figures 2 and 3) to Paris. Finally, low NH_3 concentrations
531 are measured when air masses originated from ocean regions passing through continental areas
532 with minor NH_3 sources in spring (clusters 1, 6 and 7, Figure 10). This reflects the importance of
533 long-range transport in the NH_3 budget observed over the Paris megacity in spring.

534 To quantitatively assess the influence of meteorological parameters on the formation of $\text{PM}_{2.5}$
535 from NH_3 in the IdF region, timeseries of NH_3 total columns, $\text{PM}_{2.5}$ surface concentrations, and
536 ~~five~~ meteorological parameters (temperature at 2 m, boundary layer height, total
537 precipitation, ~~and~~ relative humidity, and wind field) derived from ECMWF - ERA-~~Interim-5~~ [Dee

538 | et al., 2011, [Copernicus Climate Change Service \(C3S\), 2017](#)] were analyzed. To compute daily
539 | and monthly means, IASI NH₃ total columns have been averaged over IdF (black box in Figure 1),
540 | PM_{2.5} concentrations measured between 9 AM and 11 AM have been averaged over the 14
541 | stations (dark points in Figure 1), and ECMWF data have been averaged over a 300 km region
542 | around Paris (the blue box in Figure 1). Figure 124 shows all these parameters for spring 2014.

543 | We have flagged pollution episodes in both time series (PM_{2.5} and NH₃) by selecting data above
544 | 1-sigma standard deviation over the mean of the datasets from 2013 to 2016. This time period
545 | was selected to have enough IASI observations in the IdF region. Then two cases have been
546 | defined to study the temporal correlation between NH₃ and PM_{2.5}: case A in which both NH₃ and
547 | PM_{2.5} pollution episodes appear simultaneously, i.e. within the same day or 2 days apart
548 | (shaded in red in Figure 124); case B in which pollution episodes appear at least 3 days apart
549 | (shaded in blue in Figure 124). In Figure 124, a strong relationship between peaks of NH₃, PM_{2.5}
550 | and meteorological parameters can be seen. For example, between March 3rd and March 19th
551 | 2014 (case A), the boundary layer height is exceptionally low (456 m; compared to 760 m on
552 | average); the temperature is relatively low (280 K; 282 K on average); and there is no
553 | precipitation (0.01 mm/h; 0.11 mm/h on average). One note that peaks of maximum NH₃
554 | observed in IdF on March 11th and 12th are associated with air masses coming from the northern
555 | part of the domain (clusters 4 and 5 in Figure 10). In contrast, for the case B in which
556 | appearance of peaks of NH₃ and PM_{2.5} is not simultaneous, meteorological conditions are
557 | different: the boundary layer is thicker (908 m on April 23rd 2014), or temperature is higher (285
558 | K on April 11th 2014).

559 | To further investigate the influence of meteorological parameters on the pollution episodes in
560 | the IdF region, detailed analysis have been made over the whole dataset. Figure 132 shows the
561 | statistical distribution of meteorological parameters corresponding to case A, case B, and all
562 | observations. One can see that [for the whole dataset](#) the boundary layer height is significantly
563 | lower in case A (550 ± 205 m) than in case B (751 ± 276 m), and that precipitations are absent in
564 | case A (0,019 mm/h) compared to case B (0,085 mm/h). The temperature at 2 meters also
565 | differs between the two cases (case A: 278 ± 3 K; case B: 282 ± 4 K), but the humidity is almost
566 | the same (70% ± 17% versus 75% ± 18. [Results also suggest that simultaneous enhancements of](#)
567 | [NH₃ and PM_{2.5} over Paris \(cases A\) are mainly associated with wind fields dominantly coming](#)
568 | [from the Northeast part of the domain \(Figure S6\). Thus the combination of the following four](#)
569 | [meteorological parameters favors simultaneous appearances of NH₃ and of PM_{2.5} in Paris \(i.e.](#)
570 | [case A\): low surface temperatures \(5°C\), with thin boundary layers \(~500m\), rare precipitations,](#)
571 | [and northeast wind.%\). Thus the combination of the following three meteorological parameters](#)
572 | [favors simultaneous appearances of NH₃ and of PM_{2.5} in Paris \(i.e. case A\): low surface](#)
573 | [temperatures \(5°C\), with thin boundary layers \(~500m\), and rare precipitations.](#) In addition, the
574 | Wilcoxon-Mann-Whitney test ([Wilks, 2011], not shown here) indicates that each single

575 parameter has no significant influence on the NH_3 - $\text{PM}_{2.5}$ correlation. Therefore only a
576 combination of these different parameters has an impact on secondary aerosol formation from
577 NH_3 .

578 An explanation of these findings might be that anticyclonic conditions (low planetary boundary
579 layer), preventing pollutant dispersions in the lower atmosphere [Salmond and McKendry,
580 2005], along with moderate wind fields allow NH_3 plumes to be transported from rural to urban
581 regions [Petit et al., 2015]. In addition, thanks to relatively low atmospheric temperatures and a
582 moderate relative humidity, conversion of gas phase NH_3 to ammonium salts is then
583 accentuated via optimal phase equilibrium [Watson et al., 1994; Nenes et al., 1998]. Finally,
584 with the absence of rain, ammonium salts are stabilized in the aerosols.

585 Our observations are in agreement with previous studies [Bessagnet et al., 2016; Wang et al.,
586 2015], which have shown that the formation of ammonium salt needs a specific humidity of 60 -
587 70%, mainly because it corresponds to the deliquescence point of NH_4NO_3 in ambient air. This is
588 in agreement with our results since the mean of relative humidity in case A is 70%. Our results
589 also support the idea that a relatively low atmospheric temperature favor $\text{PM}_{2.5}$ formation in
590 particular since the phase equilibrium leads to NH_4NO_3 decomposition above 30 °C.

591 4. Conclusions

592 This study focuses on seasonal and inter-annual variabilities of NH_3 concentrations in a 400 km
593 radius-circle area around Paris to assess the evolution of major NH_3 agricultural sources and its
594 key role in the formation of the secondary aerosols that affect air quality over the Paris
595 megacity.

596 Thanks to 10-years and 5-years of regional NH_3 observations derived from IASI and CrIS, three
597 main regions of high NH_3 occurring between March and August were identified. Observed inter-
598 annual variabilities of NH_3 concentrations have been discussed with respect to total
599 precipitations and atmospheric temperature, showing that total precipitations are anti-
600 correlated with high NH_3 concentrations, and that mild temperature in late winter might causes
601 precocious fertilizer spreading due to advanced phenological growth stage.

602 To evaluate our knowledge on agricultural emissions in terms of intensity and both spatial and
603 temporal distributions, coincident CHIMERE model outputs have been compared to satellite
604 observations of IASI and CrIS for 2014 and 2015. The annual cycle is well reproduced by the
605 model ~~(correlation slopes of 0.98 and 0.71 between the model and IASI and CrIS, respectively)~~
606 but ~~the model~~ is only able to reproduce half of the observed atmospheric NH_3 variability.
607 Focusing on spring periods (March-April 2014 and 2015) of episodic NH_3 emissions, the two
608 independent satellite observations derived from IASI and CrIS show very similar spatial
609 distributions of high NH_3 concentrations, as well as their evolution in time. The comparison

610 between CHIMERE NH₃ columns and coincident satellite observations highlights the same
611 difference spatial patterns with a systematic underestimation of NH₃ concentrations from the
612 model over Belgium and an overestimation in the southern part of the domain (French
613 Brittany/Pays de la Loire and Plateau du Jura regions, as well as North of Switzerland).

614 Focusing on the Ile-de-France (IdF, 100 km around Paris) region, we found that air masses
615 originated from rich-NH₃ areas, mainly the northern part of the domain over Belgium and the
616 Netherlands, increase the observed NH₃ total columns measured by IASI over the urban area of
617 Paris. In this region, we also found that the CHIMERE model is able to reproduce the day-to-day
618 variability of PM_{2.5} concentrations (r² of 0.56), with however an underestimation during spring
619 pollution events, which could be due to unknown secondary aerosol formation processes.

620 To assess the link between NH₃ and PM_{2.5} over the Parisian (IdF) region, the main
621 meteorological parameters driving the optimal conditions involved in the PM_{2.5} formation have
622 been identified. The results show that relatively low temperature, thin boundary layer, coupled
623 with almost no precipitation and wind coming from the northeast, favor the PM_{2.5} formation
624 with the presence of atmospheric NH₃ in the IdF region. Based on a more observational
625 approach over large time scale, this work is in agreement with previous studies.

626 This study highlights the need for a better representative NH₃ monitoring to improve numerical
627 simulation of spatial and temporal NH₃ variabilities, especially at fine scales. In order to
628 compare IASI and CrIS data in absolute values, it would be recommended to derive both
629 datasets using the same retrieval algorithm. Thus, by combining these datasets bi-daily NH₃
630 total columns in absolute values at regional scale would be provided. This would help inferring
631 variability of top-down NH₃ emissions. Complementarily, long term quantification of NH₃ diurnal
632 cycle inside Paris would improve comparisons with local PM_{2.5} needed to understand secondary
633 aerosols formations. For this purpose, an ongoing activity consists in the deployment of a mini-
634 DOAS instrument [Volten et al., 2012] used for long-term and continuous monitoring of
635 atmospheric NH₃ concentrations in the center of Paris from the QUALAIR platform
636 ([https://www.ipsl.fr/en/Our-research/Atmospheric-chemistry-and-air-quality/Tropospheric-
637 chemistry/QUALAIR](https://www.ipsl.fr/en/Our-research/Atmospheric-chemistry-and-air-quality/Tropospheric-chemistry/QUALAIR)). Finally, the geostationary-orbit sounder IRS-MTG ([Stuhlmann et al.,
638 2005], to be launched after 2022) will provide NH₃ columns at very high sampling rate (every 0.5
639 hour over Europe) with an unprecedented spatial resolution (pixel size of 4 km).

640
641 Author contribution:
642 CV wrote the paper with contributions of all coauthors. CV and CC designed the study. MV, LC,
643 and SW performed IASI retrievals and ED, MWS, and KEC performed the CrIS retrievals. FM ran
644 the CHIMERE simulations. CV and TW analyzed the data with guidance from CC and PFC. All
645 authors discussed the results and contributed to the final paper.

646 Acknowledgement:

647 IASI is a joint mission of Eumetsat and the Centre National d'Etudes Spatiales (CNES, France).
648 This work was supported by the CNES. It is based on observations with IASI embarked on
649 Metop. The IASI Level-1C data are distributed in near real time by Eumetsat through the
650 EumetCast system distribution. The authors acknowledge the Aeris data infrastructure
651 (<http://iasi.aeris-data.fr/NH3/>) for providing access to the IASI Level-1C data and Level-2 NH₃
652 data used in this study. The French scientists are grateful to CNES (TOSCA) and Centre National
653 de la Recherche Scientifique (CNRS) for financial support. The research in Belgium is also funded
654 by the Belgian State Federal Office for Scientific, Technical and Cultural Affairs and the European
655 Space Agency (ESA Prodex IASI Flow project). The CrIS Fast Physical Retrieval (CFPR) NH₃ data is
656 provide through a joint collaboration between Environment and Climate Change Canada (ECCC)
657 and Atmospheric and Environmental Research (AER), Inc. (USA). The Level 1 and Level 2 input
658 data for CFPR were obtained from the University of Wisconsin-Madison Space Science and
659 Engineering Center (SSEC) and the NOAA Comprehensive Large Array-Data Stewardship System
660 (CLASS) (Liu et al.,2014), with special thanks to Axel Graumann (NOAA).

661

662 References

663 Battye, W., Aneja, V. P., and Schlesinger W. H.: Is nitrogen the next carbon?, *Earth's Future*, 5,
664 894–904, doi:10.1002/2017EF000592, 2017.

665 Beer, R., Shephard, M. W., Kulawik, S. S., Clough, S. A., Eldering, A., Bowman, K. W., Sander, S.
666 P., Fisher, B. M., Payne, V. H., Luo, M., Osterman, G. B., and Worden, J. R.: First satellite
667 observations of lower tropospheric ammonia and methanol, *Geophys. Res. Lett.*, 35, L09801,
668 doi:10.1029/2008GL033642, 2008.

669 Behera, S. N., Sharma, M., Aneja, V. P., and Balasubramanian, R.: Ammonia in the atmosphere: a
670 review on emission sources, atmospheric chemistry and deposition on terrestrial bodies, *Environ.*
671 *Sci. Pollut. Res. Int.*, 20, 8092-8131, doi: 10.1007/s11356-013-2051-9, 2013.

672 Bessagnet, B., Meleux, F., Favez, O., Beauchamp, M., Colette, A., Couvidat, F., Rouil, L., Menut,
673 L. : Le rôle de l'agriculture sur les concentrations en particules dans l'atmosphère et l'apport de
674 la modélisation (the role of agriculture on the concentrations of particles in the atmosphere and
675 supply modeling), *Pollution atmosphérique, climat, santé, société*, 229–230, 154–165, 2016.

676 Bey, I., Jacob, D. J., Yantosca, R. M., Logan, J. A., Field, B., Fiore, A. M., Li, Q., Liu, H., Mickley, L.
677 J., and Schultz, M.: Global modeling of tropospheric chemistry with assimilated meteorology:
678 Model description and evaluation, *J. Geophys. Res.*, 106, 23,073-23,096, 2001.

679 Clerbaux, C., Boynard, A., Clarisse, L., George, M., Hadji-Lazaro, J., Herbin, H., Hurtmans, D.,
680 Pommier, M., Razavi, A., Turquety, S., Wespes, C., and Coheur, P.-F.: Monitoring of atmospheric
681 composition using the thermal infrared IASI/MetOp sounder, *Atmos. Chem. Phys.*, 9, 6041–
682 6054, doi:10.5194/acp-9-6041-2009,2009

683 CEIP, Centre on Emission Inventories and Projections, ‘EMEP officially reported emission data’,
684 http://www.ceip.at/ms/ceip_home1/ceip_home/webdab_emepdatabase/reported_emissiondata/,
685 last access July 2018.

686 CITEPA, Centre Interprofessionnel Technique d'Etudes de la Pollution Atmosphérique, Format
687 SECTEN, <https://www.citepa.org/fr/air-et-climat/polluants/aep-item/ammoniac>, last access
688 April 2018.

689 Clarisse, L., Clerbaux, C., Dentener, F., Hurtmans, D., and Coheur, P.-F.: Global ammonia
690 distribution derived from infrared satellite observations, *Nat. Geosci.*, 2, 479–483,
691 <https://doi.org/10.1038/ngeo551>, 2009.

692 Clarisse, L., Shephard, M., Dentener, F., Hurtmans, D., Cady-Pereira, K., Karagulian, F., Van
693 Damme, M., Clerbaux, C., and Coheur, P.-F.: Satellite monitoring of ammonia: A case study of
694 the San Joaquin Valley, *J. Geophys. Res.*, 115, D13302, <https://doi.org/10.1029/2009JD013291>,
695 2010.

696 [Copernicus Climate Change Service \(C3S\): ERA5: Fifth generation of ECMWF atmospheric](https://cds.climate.copernicus.eu/cdsapp#!/home)
697 [reanalyses of the global climate . Copernicus Climate Change Service Climate Data Store \(CDS\),](https://cds.climate.copernicus.eu/cdsapp#!/home)
698 [date of access. https://cds.climate.copernicus.eu/cdsapp#!/home, 2017.](https://cds.climate.copernicus.eu/cdsapp#!/home)

699 Couvidat, F., Bessagnet, B., Garcia-Vivanco, M., Real, E., Menut, L., and Colette, A.: Development
700 of an inorganic and organic aerosol model (CHIMERE 2017 β v1.0): seasonal and spatial
701 evaluation over Europe, *Geosci. Model Dev.*, 11, 165-194, [https://doi.org/10.5194/gmd-11-165-](https://doi.org/10.5194/gmd-11-165-2018)
702 2018, 2018.

703 Corso, M. Medina, S., and Tillier, C. : Quelle est la part des pics de pollution dans les effets à
704 court terme de la pollution de l’air sur la santé dans les villes de France ? Saint-Maurice: Santé
705 publique France, ISBN : 979-10-289-0259-9, 2016.

706 Dammers, E., Palm, M., Van Damme, M., Vigouroux, C., Smale, D., Conway, S., Toon, G. C.,
707 Jones, N., Nussbaumer, E., Warneke, T., Petri, C., Clarisse, L., Clerbaux, C., Hermans, C., Lutsch,
708 E., Strong, K., Hannigan, J. W., Nakajima, H., Morino, I., Herrera, B., Stremme, W., Grutter, M.,
709 Schaap, M., Wichink Kruit, R. J., Notholt, J., Coheur, P.-F., and Erisman, J. W.: An evaluation of
710 IASI-NH₃ with ground-based Fourier transform infrared spectroscopy measurements, *Atmos.*
711 *Chem. Phys.*, 16, 10351–10368, <https://doi.org/10.5194/acp-16-10351-2016>, 2016.

712 Dammers, E., Shephard, M. W., Palm, M., Cady-Pereira, K., Capps, S., Lutsch, E., Strong, K.,
713 Hannigan, J. W., Ortega, I., Toon, G. C., Stremme, W., Grutter, M., Jones, N., Smale, D., Siemons,
714 J., Hrpcek, K., Tremblay, D., Schaap, M., Notholt, J., and Erisman, J. W.: Validation of the CrIS fast
715 physical NH₃ retrieval with ground-based FTIR, *Atmos Meas Tech*, 10, 2645-2667, 10.5194/amt-
716 10-2645-2017, 2017.

717 Dee, D. P., Uppala, S. M., Simmons, A. J., Berrisford, P., Poli, P., Kobayashi, S., Andrae, U.,
718 Balmaseda, M. A., Balsamo, G., Bauer, P., Bechtold, P., Beljaars, A. C. M., van de Berg, L., Bidlot,
719 J., Bormann, N., Delsol, C., Dragani, R., Fuentes, M., Geer, A. J., Haimberger, L., Healy, S. B.,
720 Hersbach, H., Hólm, E. V., Isaksen, I., Kållberg, P., Köhler, M., Matricardi, M., McNally, A. P.,
721 Monge-Sanz, B. M., Morcrette, J.-J., Park, B.-K., Peubey, C., de Rosnay, P., Tavolato, C., Thépaut,
722 J.-N. and Vitart, F.: The ERA-Interim reanalysis: configuration and performance of the data
723 assimilation system. *Q.J.R. Meteorol. Soc.*, 137: 553–597. doi: 10.1002/qj.828, 2011.

724 Erisman, J. W., Sutton, M. A., Galloway, J. N., Klimont, Z., and Winiwarter, W.: How a century of
725 ammonia synthesis changed the world, *Nat. Geosci.*, 1, 636–639, doi:10.1038/ngeo325, 2008.

726 Fortems-Cheiney, A., Dufour, G., Hamaoui-Laguel, L., Foret, G., Siour, G., Van Damme, M.,
727 Meleux, F., Coheur, P.-F., Clerbaux, C., Clarisse, L., Favez, O., Wallasch, M., and Beekmann, M.:
728 Unaccounted variability in NH₃ agricultural sources detected by IASI contributing to European
729 spring haze episode, *Geophys. Res. Lett.*, 43, 5475–5482, doi:10.1002/2016GL069361, 2016.

730 Fuzzi, S., Baltensperger, U., Carslaw, K., Decesari, S., Denier van der Gon, H., Facchini, M. C.,
731 Fowler, D., Koren, I., Langford, B., Lohmann, U., Nemitz, E., Pandis, S., Riipinen, I., Rudich, Y.,
732 Schaap, M., Slowik, J. G., Spracklen, D. V., Vignati, E., Wild, M., Williams, M., and Gilardoni, S.:
733 Particulate matter, air quality and climate: lessons learned and future needs, *Atmos. Chem.*
734 *Phys.*, 15, 8217-8299, <https://doi.org/10.5194/acp-15-8217-2015>, 2015.

735 Galloway, J. N., Aber, J. D., Erisman, J. W., Seitzinger, S. P., Howarth, R. W., Cowling, E. B., and
736 Cosby, B. J.: The Nitrogen Cascade, *BioScience*, 53, doi: 10.1641/0006-3568(2003), 2003.

737 Gong, L., Lewicki, R., Griffin, R. J., Tittel, F.K., Lonsdale, C. R., Stevens, R. G., Pierce, J. R., Malloy,
738 Q. G. J., Travis, S. A., Bobmanuel, L. M., Lefer, B. L., and Flynn, J. H.: Role of atmospheric
739 ammonia in particulate matter formation in Houston during summertime, *Atmos. Environ*, 77:
740 893–900, <https://doi.org/10.1016/j.atmosenv.2013.04.079>, 2013.

741 Hamaoui-Laguel, L., Meleux, F., Beekmann, M., Bessagnet, B., Générumont, S., Cellier, P.,
742 Létinois, L.: Improving ammonia emissions in air quality modelling for France, *Atmos. Environ.*,
743 92, 584–595, doi:10.1016/j.atmosenv.2012.08.002, 2014.

744 Heald, C. L., Collett Jr., J. L., Lee, T., Benedict, K. B., Schwandner, F. M., Li, Y., Clarisse, L.,
745 Hurtmans, D. R., Van Damme, M., Clerbaux, C., Coheur, P.-F., Philip, S., Martin, R. V., and Pye, H.
746 O. T.: Atmospheric ammonia and particulate inorganic nitrogen over the United States, *Atmos.*
747 *Chem. Phys.*, 12, 10295–10312, doi:10.5194/acp-12-10295-2012, 2012.

748 [Hernández, D. L., Vallano, D. M., Zavaleta, E. S., Tzankova, Z., Pasari, J. R., Weiss, S., Selmants, P.](#)
749 [C., and Morozumi, C.: Nitrogen Pollution Is Linked to US Listed Species Declines, *BioScience*, 66](#)
750 [\(3\), 213–222, <https://doi.org/10.1093/biosci/biw003>, 2016.](#)

751 Holland, E. A., Bertman, S. B., Carroll, M. A., Guenther, A. B., Shepson, P. B., Sparks, J. P., and
752 Lee-Taylor, J.: U.S. Nitrogen Science Plan Focuses Collaborative Efforts, *Eos. Trans. Am. Geophys.*
753 *Union.*, 86(27), 253-260, 2005.

754 [Isbell F., Reich, P. B., Tilman, D., Hobbie, S. E., Polasky, S., and Binder S.: Nutrient enrichment,](#)
755 [biodiversity loss, and consequent declines in ecosystem productivity, *PNAS*, 110 \(29\), 11911-](#)
756 [11916, <https://doi.org/10.1073/pnas.1310880110>, 2013.](#)

757 Kaiser, J. W., Heil, A., Andreae, M. O., Benedetti, A., Chubarova, N., Jones, L., Morcrette, J.-J.,
758 Razinger, M., Schultz, M. G., Suttie, M., and van der Werf, G. R.: Biomass burning emissions
759 estimated with a global fire assimilation system based on observed fire radiative power. *BG*,
760 9:527-554, 2012.

761 Kharol, S. K., M. W. Shephard, C. A. McLinden, L. Zhang, C. E. Sioris, J. M. O'Brien, R. Vet, K. E.
762 Cady-Pereira, E. Hare, J. Siemons, and N. A. Krotkov.: Dry deposition of reactive nitrogen from
763 satellite observations of ammonia and nitrogen dioxide over North America, *Geophysical*
764 *Research. Letters*, 45, 1157-1166, <https://doi.org/10.1002/2017GL075832>, 2018.

765

766 Kranenburg, R., Hendriks, C., Kuenen, J., and Schaap, M.: Improved Modelling of Ammonia by
767 Using Manure Transport Data, In International Technical Meeting on Air Pollution Modelling and
768 its Application (pp. 483-486). Springer, Cham, December 2016.

769

770 Kuenen, J. J. P., Visschedijk, A. J. H., Jozwicka, M., and Denier van der Gon, H. A. C.: TNO-
771 MACC_II emission inventory; a multi-year (2003–2009) consistent high-resolution European
772 emission inventory for air quality modelling, *Atmos. Chem. Phys.*, 14, 10963-10976,
773 <https://doi.org/10.5194/acp-14-10963-2014>, 2014.

774

775 Li, Y., Thompson, T. M., Van Damme, M., Chen, X., Benedict, K. B., Shao, Y., Day, D., Boris, A.,
776 Sullivan, A. P., Ham, J., Whitburn, S., Clarisse, L., Coheur, P.-F., and Collett Jr., J. L.: Temporal and
777 spatial variability of ammonia in urban and agricultural regions of northern Colorado, United
778 States, *Atmos. Chem. Phys.*, 17, 6197-6213, <https://doi.org/10.5194/acp-17-6197-2017>, 2017.

779

780 Mailler, S., Menut, L., Khvorostyanov, D., Valari, M., Couvidat, F., Siour, G., Turquety, S., Briant,
781 R., Tuccella, P., Bessagnet, B., Colette, A., Letinois, L., and Meleux, F.: CHIMERE-2017: from
782 urban to hemispheric chemistry-transport modeling, *Geosci. Model Dev.*, 10, 2397-2423,
783 <https://doi.org/10.5194/gmd-10-2397-2017>, 2017.

784 Menut, L., Bessagnet, B., Khvorostyanov, D., Beekmann, M., Blond, N., Colette, A., Coll, I., Curci,
785 G., Foret, G., Hodzic, A., Mailler, S., Meleux, F., Monge, J.L., Pison, I., Siour, G., Turquety, S.,
786 Valari, M., Vautard, R., and Vivanco, M.G.: CHIMERE 2013: a model for regional atmospheric
787 composition modelling, *Geosci. Model Dev.*, 6, 981-1028, doi:10.5194/gmd-6-981-2013, 2013.

788 Moran, M. D., Dastoor, A., and Morneau, G.: Long-Range Transport of Air Pollutants and
789 Regional and Global Air Quality Modelling. In: Taylor E., McMillan A. (eds) *Air Quality*
790 *Management*, Springer, Dordrecht, 2014.

791 Moncet, J.-L., Uymin G., Lipton A. E., and Snell H. E.: Infrared radiance modeling by optimal
792 spectral sampling, *J. Atmos. Sci.*, 65, 3917-3934, <https://doi.org/10.1175/2008JAS2711.1>, 2008.

793 Myhre, G., Samset, B. H., Schulz, M., Balkanski, Y., Bauer, S., Bernsten, T. K., Bian, H., Bellouin,
794 N., Chin, M., Diehl, T., Easter, R. C., Feichter, J., Ghan, S. J., Hauglustaine, D., Iversen, T., Kinne,
795 S., Kirkevåg, A., Lamarque, J.-F., Lin, G., Liu, X., Lund, M. T., Luo, G., Ma, X., van Noije, T., Penner,
796 J. E., Rasch, P. J., Ruiz, A., Seland, Ø., Skeie, R. B., Stier, P., Takemura, T., Tsigaridis, K., Wang, P.,
797 Wang, Z., Xu, L., Yu, H., Yu, F., Yoon, J.-H., Zhang, K., Zhang, H., and Zhou, C.: Radiative forcing of
798 the direct aerosol effect from AeroCom Phase II simulations, *Atmos. Chem. Phys.*, 13, 1853-
799 1877, <https://doi.org/10.5194/acp-13-1853-2013>, 2013.

800 [Nenes, A.; Pandis, S. N.; Pilinis, C.: ISORROPIA: A New Thermodynamic Equilibrium Model for](#)
801 [Multiphase Multicomponent Inorganic Aerosols. *Aquat. Geoch.*, 4, 123-152, 1998.](#)

802 National Emission Ceilings Directive (NEC) reporting status, doi:10.2800/984979,
803 [https://www.eea.europa.eu/themes/air/national-emission-ceilings/nec-directive-reporting-](https://www.eea.europa.eu/themes/air/national-emission-ceilings/nec-directive-reporting-status-2018)
804 [status-2018](#), 2018.

805 Nenes, A.; Pandis, S. N.; Pilinis, C.: ISORROPIA: A New Thermodynamic Equilibrium Model for
806 Multiphase Multicomponent Inorganic Aerosols. *Aquat. Geoch.*, 4, 123-152, 1998.

807 Nowak, J. B., Neuman, J. A., Bahreini, R., Middlebrook, A. M., Holloway, J. S., McKeen, S. A.,
808 Parrish, D. D., Ryerson, T. B., and Trainer, M.: Ammonia sources in the California South Coast Air
809 Basin and their impact on ammonium nitrate formation, *Geophys. Res. Lett.*, 39, L07804,
810 <https://doi.org/10.1029/2012GL051197>, 2012.

811 Petetin, H., Sciare, J., Bressi, M., Gros, V., Rosso, A., Sanchez, O., Sarda-Estève, R., Petit, J.-E.,
812 and Beekmann, M.: Assessing the ammonium nitrate formation regime in the Paris megacity

813 and its representation in the CHIMERE model, *Atmos. Chem. Phys.*, 16, 10419-10440,
814 <https://doi.org/10.5194/acp-16-10419-2016>, 2016.

815 Petit, J.-E., Favez, O., Sciare, J., Crenn, V., Sarda-Estève, R., Bonnaire, N., Močnik, G., Dupont, J.-
816 C., Haeffelin, M., and Leoz-Garziandia, E.: Two years of near real-time chemical composition of
817 submicron aerosols in the region of Paris using an Aerosol Chemical Speciation Monitor (ACSM)
818 and a multi-wavelength Aethalometer, *Atmos. Chem. Phys.*, 15, 2985-3005,
819 <https://doi.org/10.5194/acp-15-2985-2015>, 2015.

820 [Petit, J.-E., Amodeo, T., Meleux, F., Bessagnet, B., Menut, L., Grenier, D., Pellan, Y., Ockler, A.,
821 Rocq, B., Gros, V., Sciare, J., and Favez, O.: Characterising an intense PM pollution episode in
822 March 2015 in France from multi-site approach and near real time data: Climatology,
823 variabilities, geographical origins and model evaluation, *Atmospheric Environment, Volume 155*,
824 <https://doi.org/10.1016/j.atmosenv.2017.02.012>, 2017.](https://doi.org/10.1016/j.atmosenv.2017.02.012)

825 Pinder, R. W., Adams, P. J., Pandis, S.N., and Gilliland, A. B.: Temporally resolved ammonia
826 emission inventories: current estimates, evaluation tools, and measurement needs, *J. Geophys.*
827 *Res.*, 111, D16310, <http://dx.doi.org/10.1029/2005JD006603>, 2006.

828 Pope III, C. A., Ezzati M., and Dockery, D. W.: Fine-particulate air pollution and life expectancy in
829 the United States, *New England J. Med.*, 360 (4), 376-386, 2009.

830 Ramanantenasoa, M. M. J., Gilliot, J.-M., Mignolet, C., Bedos, C., Mathias, E., Eglin, T.,
831 Makowski, D., and Générumont, S.: A new framework to estimate spatio-temporal ammonia
832 emissions due to nitrogen fertilization in France, *Science of The Total Environment*, 645, 205 –
833 219, <https://doi.org/10.1016/j.scitotenv.2018.06.202>, 2018.

834 [Robinson, T. P., Wint, G. R. W., Conchedda, G., Van Boeckel, T. P., Ercoli, V., Palamara, E., Cinardi,
835 G., D'Aiotti, L., Hay, S., and Gilbert, M.: Mapping the global distribution of livestock, *PLoS One*,
836 9\(5\): e96084, <https://doi.org/10.1371/journal.pone.0096084>, 2014.](https://doi.org/10.1371/journal.pone.0096084)

837 Rockström, J., Steffen, W., Noone, K., Persson, A., Chapin Iii, F. S., Lambin, E. F., Lenton, T. M.,
838 Scheffer, M., Folke, C., Schellnhuber, H. J., Nykvist, B., de Wit, C. A., Hughes, T., van der Leeuw,
839 S., Rodhe, H., Sörlin, S., Snyder, P. K., Costanza, R., Svedin, U., Falkenmark, M., Karlberg, L.,
840 Corell, R. W., Fabry, V. J., Hansen, J., Walker, B., Liverman, D., Richardson, K., Crutzen, P., and
841 Foley, J. A.: Planetary boundaries: Exploring the safe operating space for humanity, *Ecology and
842 Society*, 14, 2009.

843 Rodgers, C. D.: *Inverse Methods for Atmospheric Sounding: Theory and Practice*, vol. 2 of Series
844 on Atmospheric, Oceanic and Planetary Physics, edited by: Taylor, F. W., World Scientific, 2000.

845 Salmond, J. A., and McKendry, I. G.: A Review of Turbulence in the Very Stable Nocturnal
846 Boundary Layer and Its Implications for Air Quality, *Progress in Physical Geography*, 29 (2), 171–
847 188, 2005.

848 [Scarlat, N., Fahl, F., Dallemand, J.-F., Monforti, F., and Motola, V.: A spatial analysis of biogas
849 potential from manure in Europe. *Renew. Sustain. Energy Rev.*, 94, 915–930,
850 <https://doi.org/10.1016/j.rser.2018.06.035>, 2018.](#)

851 Schaap, M., Timmermans, R., Roemer, M., Boersen, G., Builtjes, P., Sauter, F., Velders, G., and
852 Beck, J.: The LOTOS-EUROS model: Description, validation and latest developments, *Int. J.*
853 *Environ. Pollut.*, 32, 270–290, doi:[10.1504/IJEP.2008.017106](https://doi.org/10.1504/IJEP.2008.017106), 2008.

854 [Schiferl, Luke D., Heald, Colette L., van Damme, Martin, Clarisse, Lieven, Clerbaux, Cathy et al.
855 Interannual variability of ammonia concentrations over the United States: sources and
856 implications. *Atmospheric Chemistry and Physics*, 16 \(18\), 12305-12328, 2016.](#)

857 Shephard, M.W., and Cady-Pereira, K.E.: Cross-track Infrared Sounder (CrIS) satellite
858 observations of tropospheric ammonia, *Atmos. Meas. Tech.*, 8, 1323-1336, 2015.

859 Shephard, M. W., Cady-Pereira, K. E., Luo, M., Henze, D. K., Pinder, R. W., Walker, J. T., Rinsland,
860 C. P., Bash, J. O., Zhu, L., Payne, V. H., and Clarisse, L.: TES ammonia retrieval strategy and global
861 observations of the spatial and seasonal variability of ammonia, *Atmos. Chem. Phys.*, 11, 10743–
862 10763, doi:10.5194/acp-11-10743-2011, 2011.

863 Skjøth, C. A., Geels, C., Berge, H., Gyldenkerne, S., Fagerli, H., Ellermann, T., Frohn, L. M.,
864 Christensen, J., Hansen, K. M., Hansen, K., and Hertel, O.: Spatial and temporal variations in
865 ammonia emissions – a freely accessible model code for Europe, *Atmos. Chem. Phys.*, 11, 5221-
866 5236, <https://doi.org/10.5194/acp-11-5221-2011>, 2011.

867 Skyllakou, K., Murphy, B. N., Megaritis, A. G., Fountoukis, C., and Pandis, S. N.: Contributions of
868 local and regional sources to fine PM in the megacity of Paris, *Atmos. Chem. Phys.*, 14, 2343-
869 2352, <https://doi.org/10.5194/acp-14-2343-2014>, 2014.

870 Sutton, M. A., Bleeker, A., Howard, C., Bekunda, M., Grizzetti, B., de Vries, W., van Grinsven, H.,
871 Abrol, Y., Adhya, T., Billen G. and Davidson, E., Datta, A., Diaz, R., Erisman, J., Liu, X., Oenema,
872 O., Palm, C., Raghuram, N., Reis, S., Scholz, R., Sims, T., Westhoek, H., Zhang, F., with
873 contributions from Ayyappan, S., Bouwman, A., Bustamante, M., Fowler, D., Galloway, J., Gavito,
874 M., Garnier, J., Greenwood, S., Hellums, D., Holland, M., Hoysall, C., Jaramillo, V., Klimont, Z.,
875 Ometto, J., Pathak, H., Plocq Fichelet, V., Powlson, D., Ramakrishna, K., Roy, A., Sanders, K.,
876 Sharma, C., Singh, B., Singh, U., Yan, X., and Zhang, Y.: Our Nutrient World: The challenge to
877 produce more food and energy with less pollution. *Global Overview of Nutrient Management*,

878 Centre for Ecology & Hydrology on behalf of the Global Partnership on Nutrient Management
879 and the International Nitrogen Initiative, 114 pp., 2013.

880 Stuhlmann, R., Rodriguez, A., Tjemkes, S., Grandell, J., Arriaga, A., Bézy, J.-L., Aminou, D., and
881 Bensi, P.: Plans for EUMETSAT's Third Generation Meteosat (MTG) Geostationary Satellite
882 Program, *Adv. Space Res.*, 36, 975–981, 2005.

883 Toro, R.A., Canales, M., Flocchini, R.G., Morales, R.G.E., and Leiva G, M.A.: Urban atmospheric
884 ammonia in Santiago City, Chile, *Aerosol Air Qual. Res.*, 14: 33–44, doi:
885 10.4209/aaqr.2012.07.0189, 2014.

886 Van Damme, M., Clarisse, L., Heald, C. L., Hurtmans, D., Ngadi, Y., Clerbaux, C., Dolman, A. J.,
887 Erisman, J. W., and Coheur, P. F.: Global distributions, time series and error characterization of
888 atmospheric ammonia (NH₃) from IASI satellite observations, *Atmos. Chem. Phys.*, 14, 2905–
889 2922, <https://doi.org/10.5194/acp-14-2905-2014>, 2014a.

890 Van Damme, M., Wichink Kruit, R. J., Schaap, M., Clarisse, L., Clerbaux, C., Coheur, P.-F.,
891 Damers, E., Dolman, A. J., and Erisman, J. W.: Evaluating four years of atmospheric ammonia
892 (NH₃) over Europe using IASI satellite observations and LOTOS-EUROS model results, *J. Geophys.*
893 *Res.-Atmos.*, 119, 9549–9566, 2014b.

894 Van Damme, M., Erisman, J. W., Clarisse, L., Damers, E., Whitburn, S., Clerbaux, C., Dolman, A.
895 J., and Coheur, P.-F.: Worldwide spatiotemporal atmospheric ammonia (NH₃) columns variability
896 revealed by satellite, *Geophys. Res. Lett.*, 42 (20), 8660–8668, 2015a.

897 Van Damme, M., Clarisse, L., Damers, E., Liu, X., Nowak, J. B., Clerbaux, C., Flechard, C. R.,
898 Galy-Lacaux, C., Xu, W., Neuman, J. A., Tang, Y. S., Sutton, M. A., Erisman, J. W., and Coheur, P.
899 F.: Towards validation of ammonia (NH₃) measurements from the IASI satellite, *Atmos. Meas.*
900 *Tech.*, 8, 1575–1591, <https://doi.org/10.5194/amt-8-1575-2015>, 2015b.

901 Van Damme, M., Whitburn, S., Clarisse, L., Clerbaux, C., Hurtmans, D., and Coheur, P.-F.: Version
902 2 of the IASI NH₃ neural network retrieval algorithm: near-real-time and reanalysed datasets,
903 *Atmos. Meas. Tech.*, 10, 4905–4914, <https://doi.org/10.5194/amt-10-4905-2017>, 2017.

904 Van Damme, M., Clarisse, L., Whitburn, S., Hadji-Lazaro J., Hurtmans, D., Clerbaux, C., and
905 Coheur, P.-F.: Industrial and agricultural ammonia point sources exposed, *Nature*, 564 (7734):
906 99, DOI: 10.1038/s41586-018-0747-1, 2018.

907 van Vuuren, D. P., Edmonds, J., Kainuma, M. et al. he Representative Concentration Pathways:
908 An overview, *Clim. Change*, 109 (1–2), 5–31, <https://doi.org/10.1007/s10584-011-0148-z>, 2011.

909 Volten, H., Bergwerff, J. B., Haaima, M., Lolkema, D. E., Berkhout, A. J. C., van der Hoff, G. R.,
910 Potma, C. J. M., Wichink Kruit, R. J., van Pul, W. A. J., and Swart, D. P. J.: Two instruments based
911 on differential optical absorption spectroscopy (DOAS) to measure accurate ammonia
912 concentrations in the atmosphere, *Atmos. Meas. Tech.*, 5, 413-427,
913 <https://doi.org/10.5194/amt-5-413-2012>, 2012.

914 Wang, S., Nan, J., Shi, C., Fu, Q., Gao, G., Wang, D., Cui, H., Saiz-Lopez A., and Zhou, B.:
915 Atmospheric ammonia and its impacts on regional air quality over the megacity of Shanghai,
916 China, *Scientific Reports*, 5, 15842, <http://dx.doi.org/10.1038/srep15842>, 2015.

917 Warner, J. X., Dickerson, R. R., Wei, Z., Strow, L. L., Wang, Y., and Liang, Q.: Increased
918 atmospheric ammonia over the world's major agricultural areas detected from space, *Geophys.*
919 *Res. Lett.*, doi: 10.1002/2016gl072305, 2017.

920 Warner, J. X., Wei, Z., Strow, L. L., Dickerson, R. R., and Nowak, J. B.: The global tropospheric
921 ammonia distribution as seen in the 13-year AIRS measurement record, *Atmos. Chem. Phys.*, 16,
922 5467-5479, <https://doi.org/10.5194/acp-16-5467-2016>, 2016.

923 Watson, J. G., Chow, J. C., Lurmann, F. W., and Musarra, S. P.: Ammonium Nitrate, Nitric Acid,
924 and Ammonia Equilibrium in Wintertime Phoenix, Arizona. *Air & Waste*, 44 (4), 405–412, 1994.

925 [Wesely, M.: Parameterization of Surface Resistances to Gaseous Dry Deposition in Regional-](#)
926 [Scale Numerical Models. *Atmospheric Environment*, 23\(23\):1293–1304, 1989.](#)

927 Whitburn, S., Van Damme, M., Clarisse, L., Bauduin, S., Heald, C., Hadji-Lazaro, J., Hurtmans, D.,
928 Zondlo, M., Clerbaux, C., and Coheur, P.-F.: A flexible and robust neural network IASI-NH₃
929 retrieval algorithm, *J. Geophys. Res. Atmos.*, 121, 6581–6599,
930 <https://doi.org/10.1002/2016JD024828>, 2016.

931 Wilks, Daniel S.: *Statistical Methods in the Atmospheric Sciences*, 3rd ed. Oxford, Waltham, MA:
932 Academic Press, 2011.

933 Ye, X., Ma, Z., Zhang, J., Du, H., Chen, J., Chen, H., Yang, X., Gao, W. and Geng, F.: Important role
934 of ammonia on haze formation in Shanghai, *Environ. Res. Lett.*, 6: 024019, doi:10.1088/1748-
935 9326/6/2/024019, 2011.

936 Zavyalov, V., Esplin, M., Scott, D., Esplin, B., Bingham, G., Hoffman, E., Lietzke, C., Predina, J.,
937 Frain, R., Suwinski, L., Han, Y., Major, C., Graham, B., and Phillips, L.: Noise performance of the
938 CrIS instrument, *J. Geophys. Res.*, doi: 10.1002/2013JD020457, 2013.

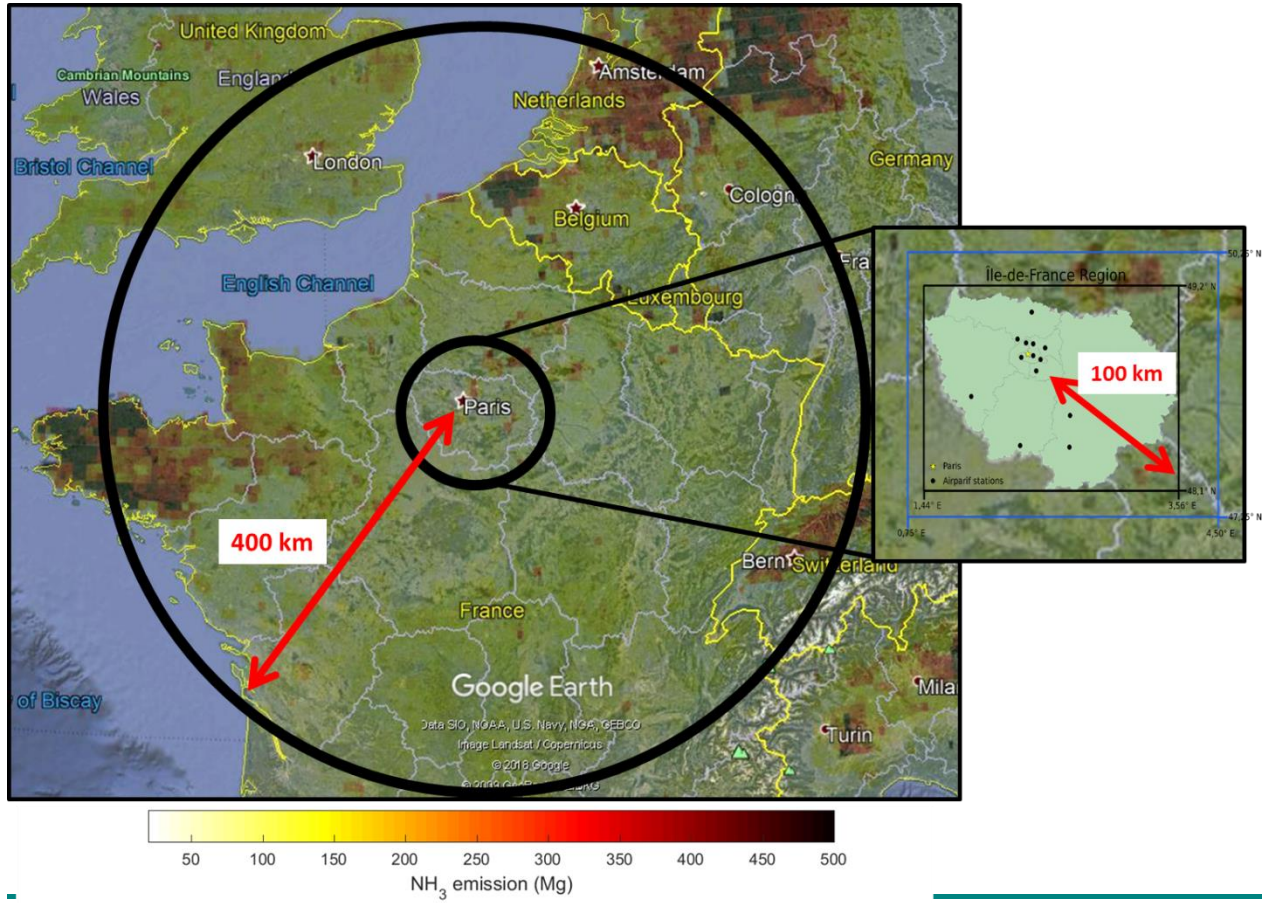
939 Zhang, Q. J., Beekmann, M., Drewnick, F., Freutel, F., Schneider, J., Crippa, M., Prevot, A. S. H.,
940 Baltensperger, U., Poulain, L., Wiedensohler, A., Sciare, J., Gros, V., Borbon, A., Colomb, A.,

941 Michoud, V., Doussin, J.-F., Denier van der Gon, H. A. C., Haeffelin, M., Dupont, J.-C., Siour, G.,
942 Petetin, H., Bessagnet, B., Pandis, S. N., Hodzic, A., Sanchez, O., Honoré, C., and Perrussel, O.:
943 Formation of organic aerosol in the Paris region during the MEGAPOLI summer campaign:
944 evaluation of the volatility-basis-set approach within the CHIMERE model, *Atmos. Chem. Phys.*,
945 13, 5767-5790, <https://doi.org/10.5194/acp-13-5767-2013>, 2013.

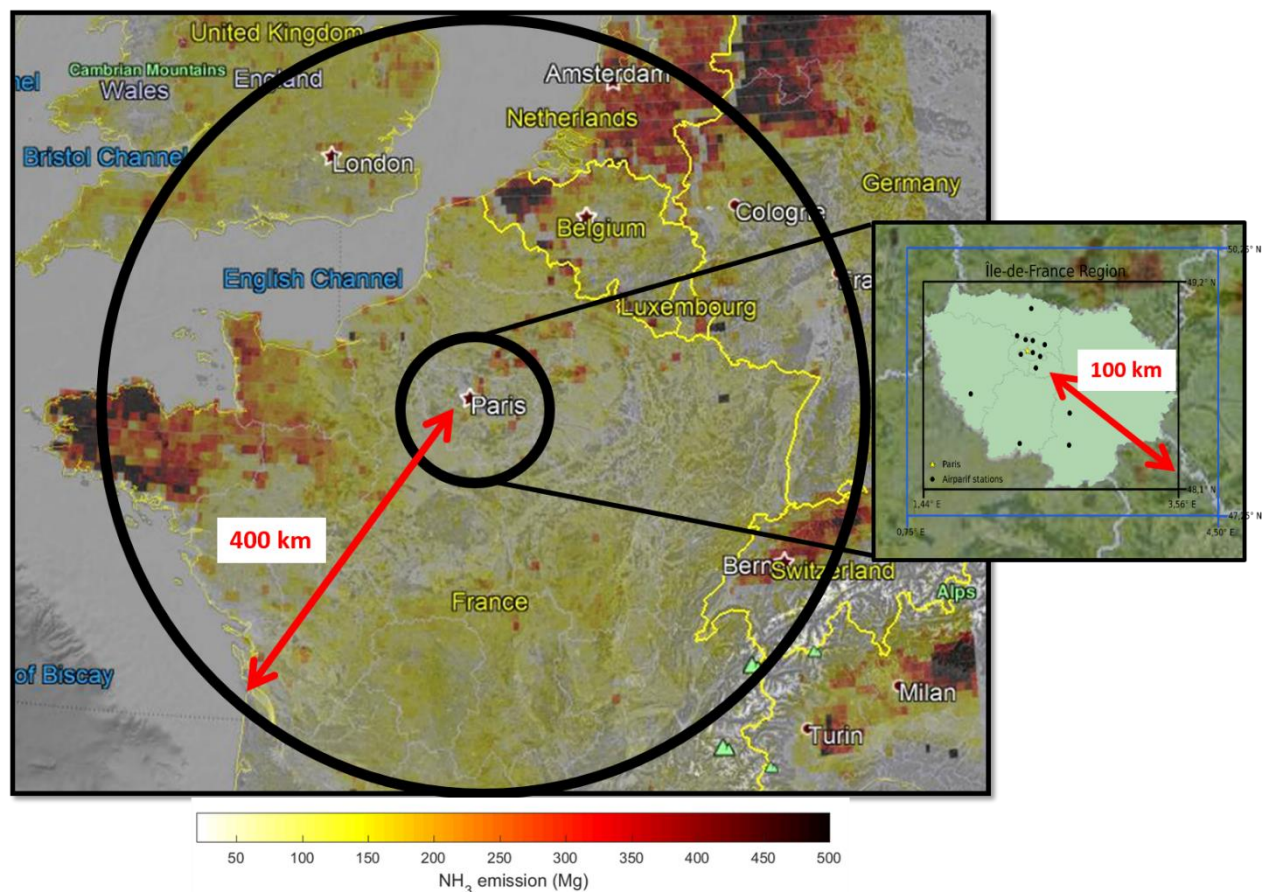
946 Zhao, M., Wang, S., Tan, J., Hua, Y., Wu, D., and Hao, J.: Variation of urban atmospheric
947 ammonia pollution and its relation with PM_{2.5} chemical property in winter of Beijing, China,
948 *Aerosol Air Qual. Res.*, 16, 1378–1389, <https://doi.org/10.4209/aaqr.2015.12.0699>, 2016.

949 Zhu, L., Henze, D. K., Cady-Pereira, K. E., Shephard, M. W., Luo, M., Pinder, R. W., Bash, J. O., and
950 Jeong, G.: Constraining U.S. ammonia emissions using TES remote sensing observations and the
951 GEOS-Chem adjoint model, *J. Geophys. Res.-Atmos.*, 118, 3355–3368, doi:10.1002/jgrd.50166,
952 2013.

FIGURES

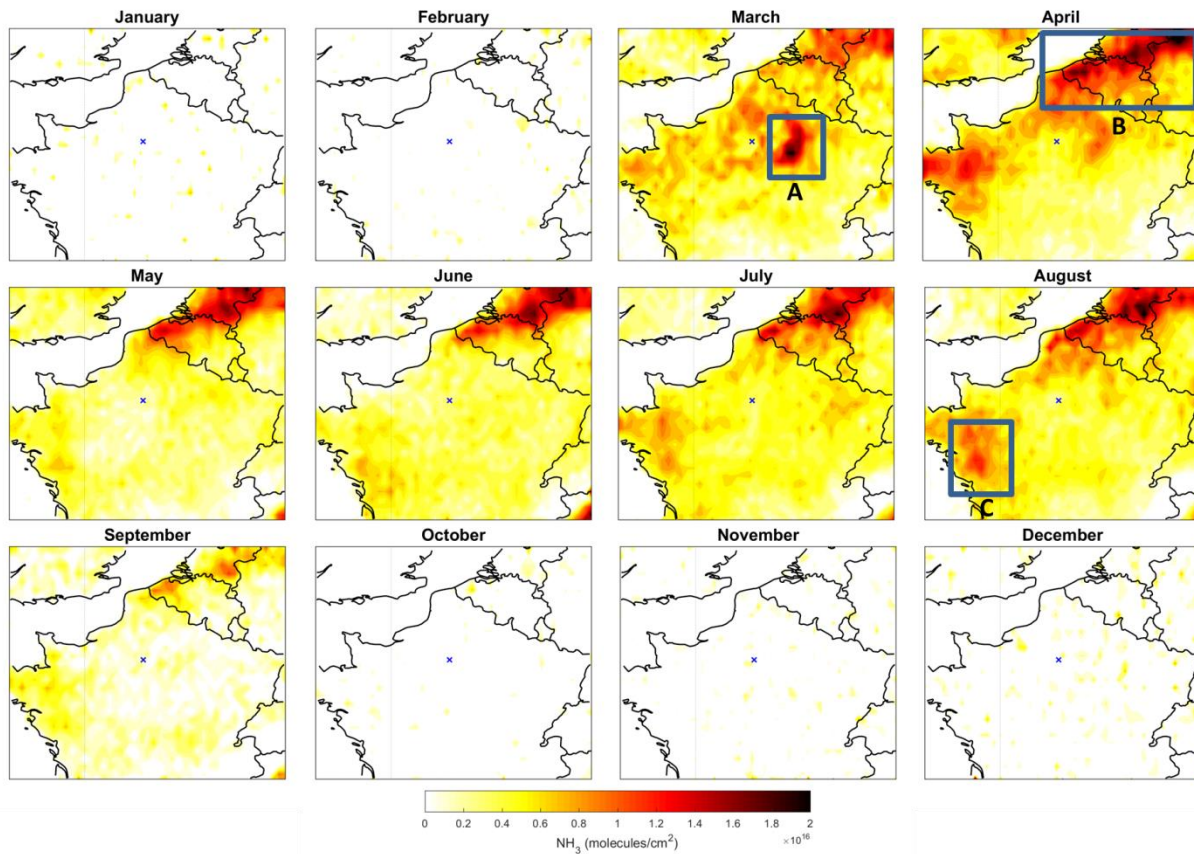


954



955

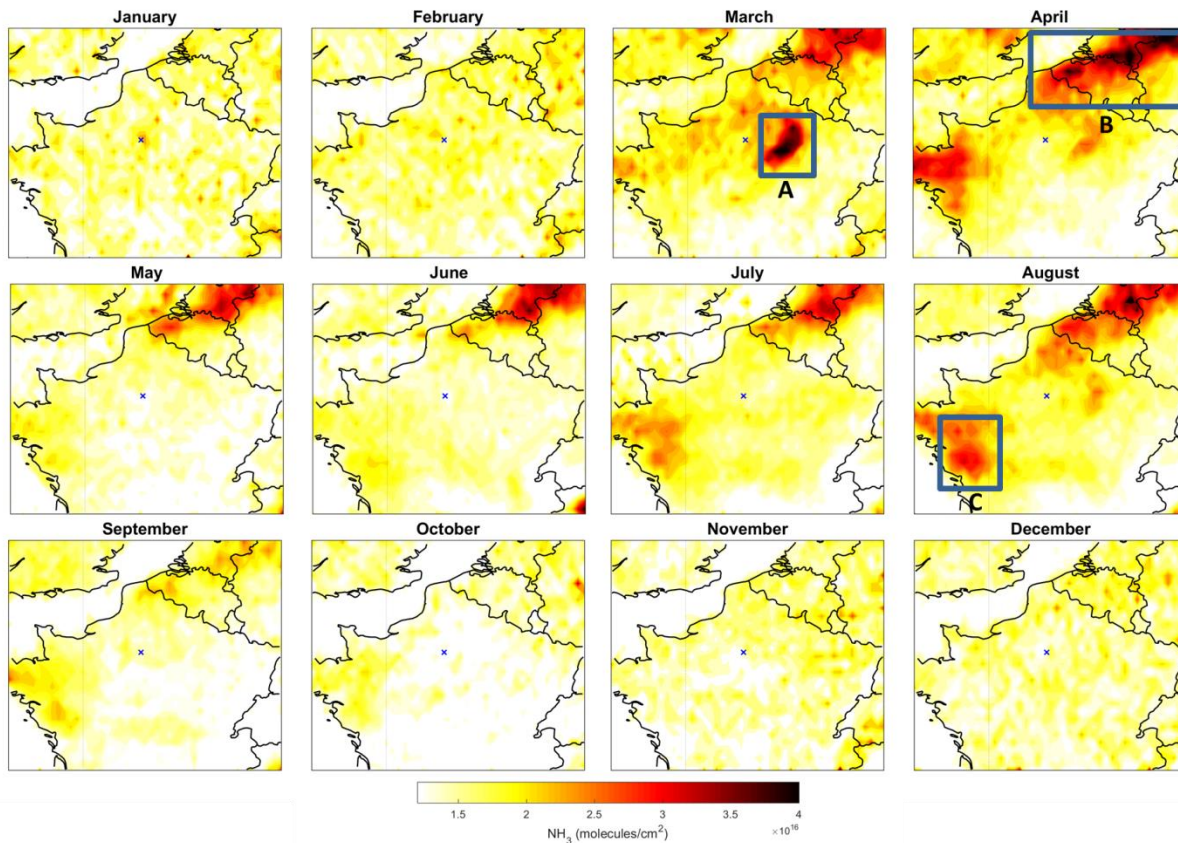
956 Figure 1: Region of analysis: 400 km radius-circle around the Paris megacity and 100 km around
 957 Paris. The latter is representative of the Ile-de-France (IdF) region where the Airparif PM
 958 observational network is located. Black points are the locations of the Airparif stations
 959 measuring hourly PM_{2.5} concentration at the surface. The black (blue) box delimitates the IdF
 960 region in which the IASI NH₃ (ECMWF) data have been considered. The overlay represents NH₃
 961 emissions (in Mg per year and per cell of 0.1°x0.1°) derived from the EMEP inventory for 2015.



962

963 Figure 2: Monthly means of NH₃ total columns (molecules/cm²) derived from 10 years (2008-
 964 2017) of IASI NH₃-retrieved columns. The blue cross indicates Paris location.

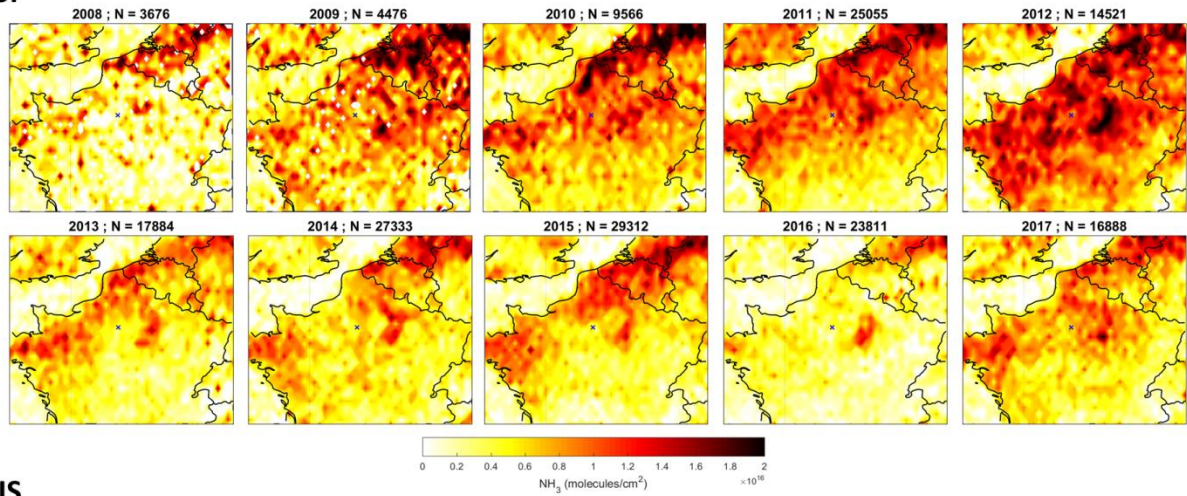
965



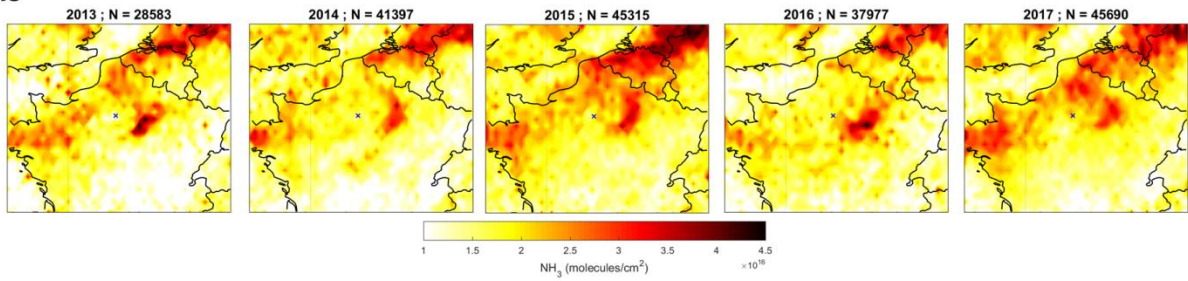
966

967 Figure 3: Monthly means of NH_3 total columns (molecules/cm^2) derived from 5 years (2013-
 968 2017) of CrIS NH_3 -retrieved columns. The blue cross indicates Paris location.

IASI

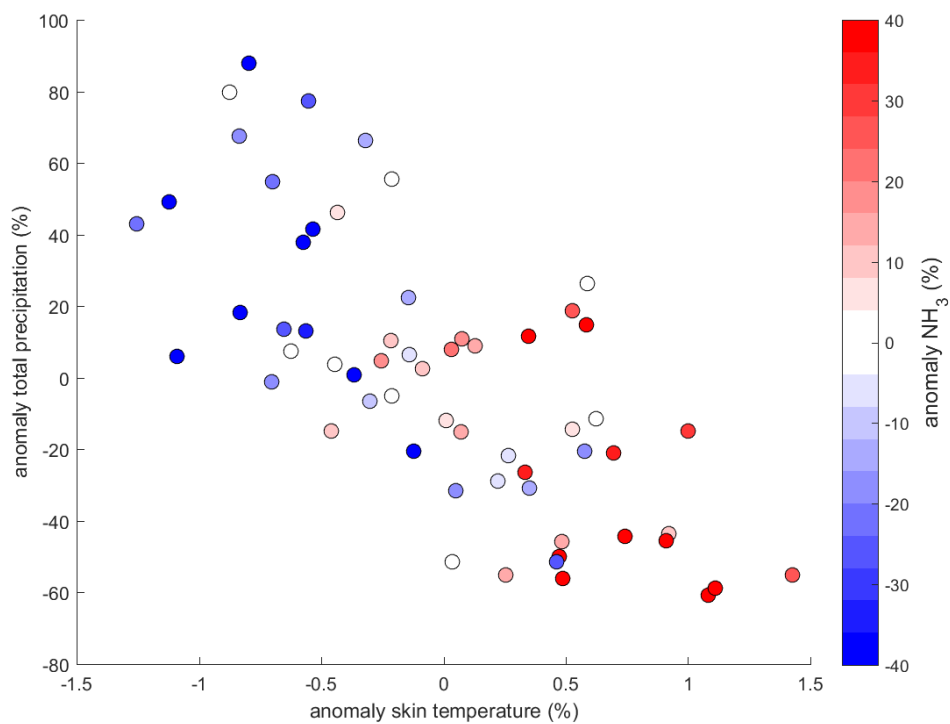


CrIS

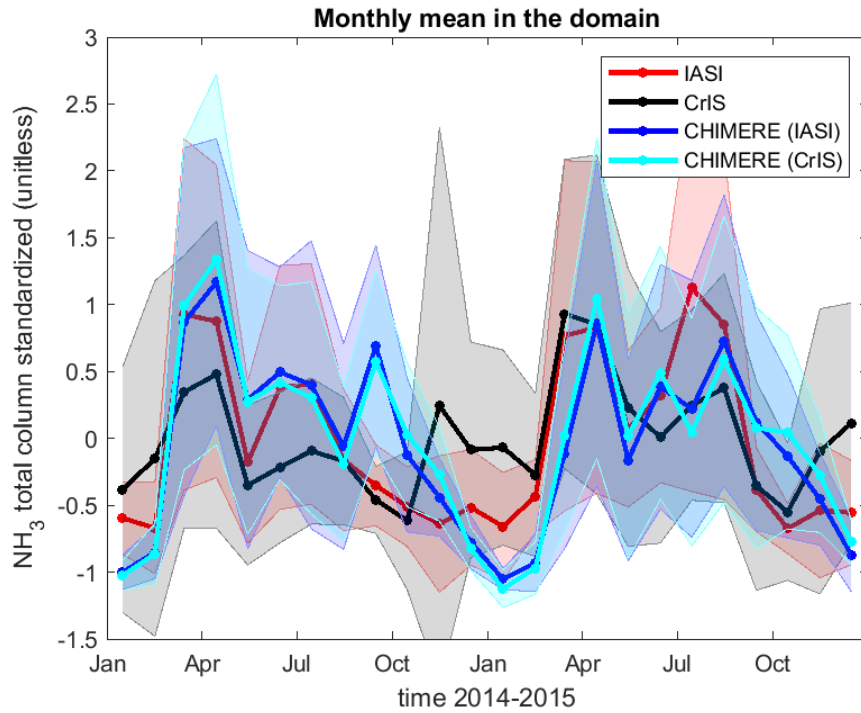


969

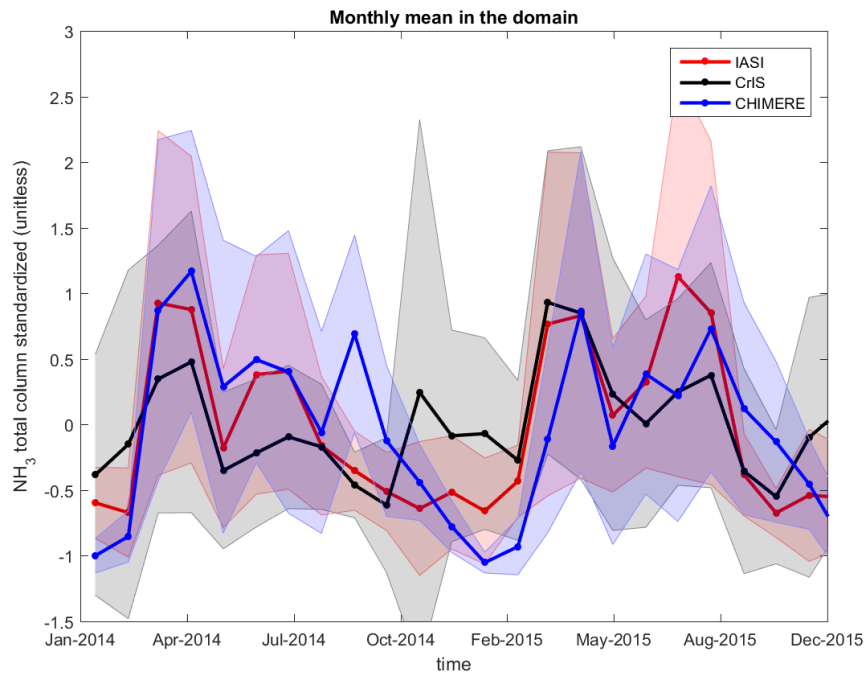
970 Figure 4: Maps of monthly mean NH₃ total columns (molecules/cm²) in March-April period
971 derived from IASI from 2008 to 2017 and CrIS from 2013 to 2017.



972
 973 Figure 5: Scatter plot of monthly mean anomaly (relative to the 10-years – 2008 to 2017 -
 974 monthly average) of total precipitation versus skin temperature derived from ECMWF from
 975 March to August in the domain, and color coded by the NH₃ total columns anomaly derived
 976 from IASI.

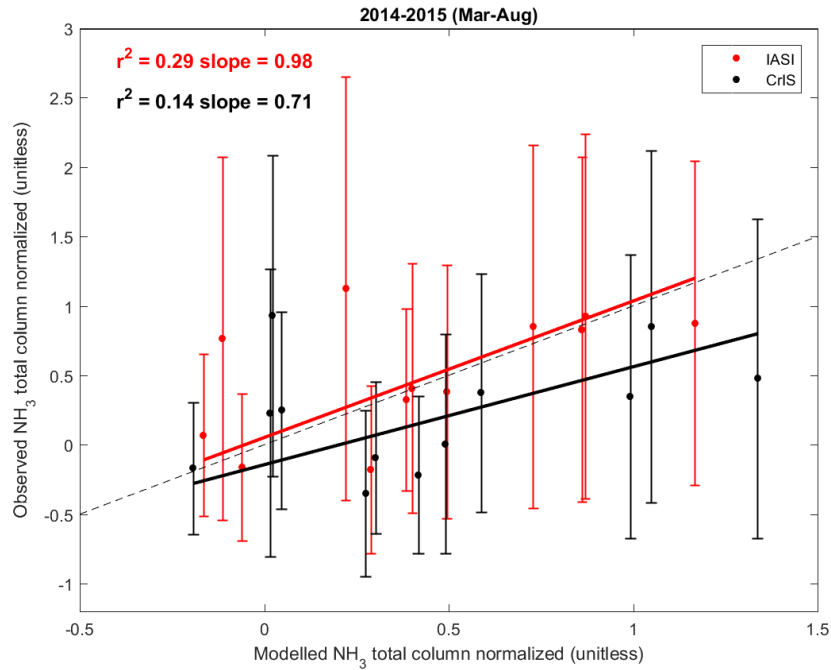


977

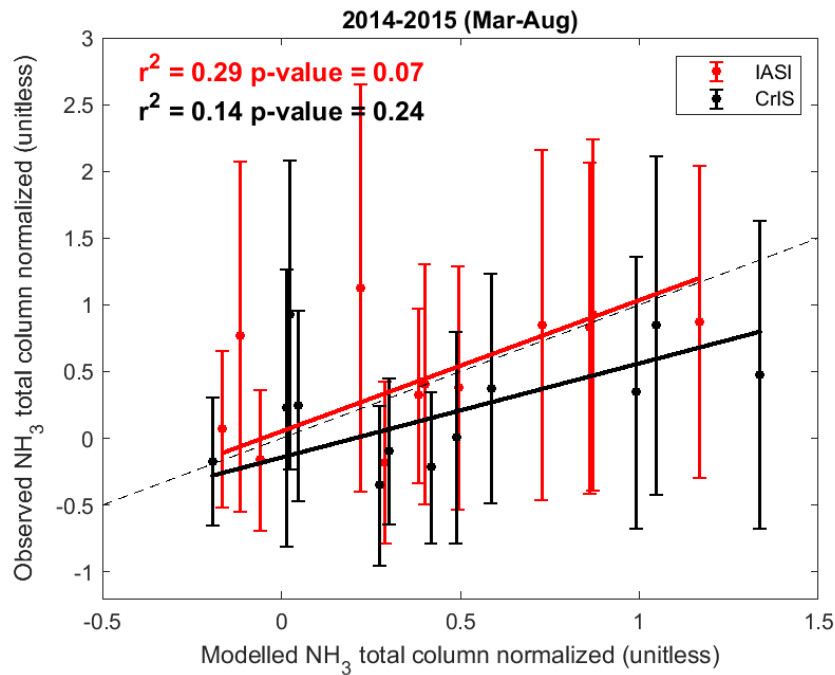


978

979 Figure 6: Standardized monthly mean concentrations derived from IASI (red), CrIS (black),
 980 CHIMERE sampled at IASI overpass time and space (blue) and CHIMERE sample at CrIS overpass
 981 time and space (cyan) for 2014 and 2015. Shaded areas correspond to the one-sigma standard
 982 deviation around the means.

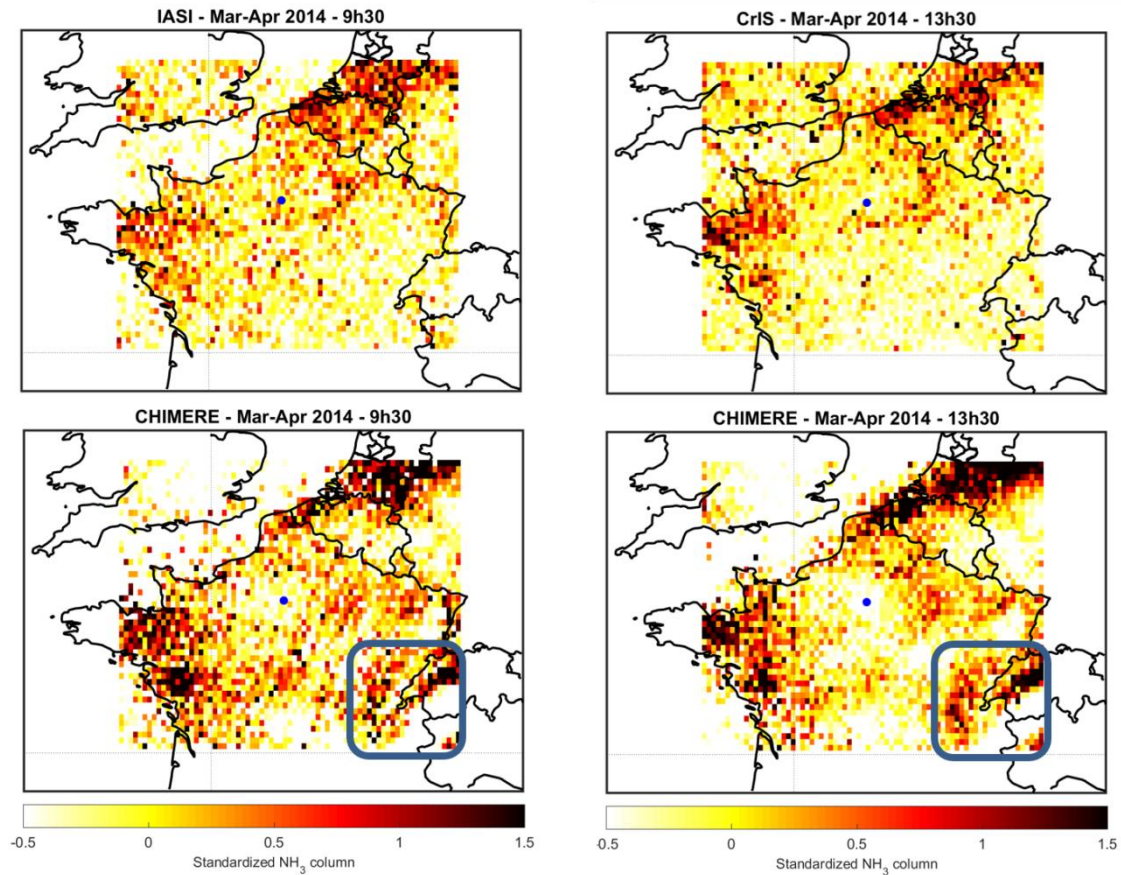


983



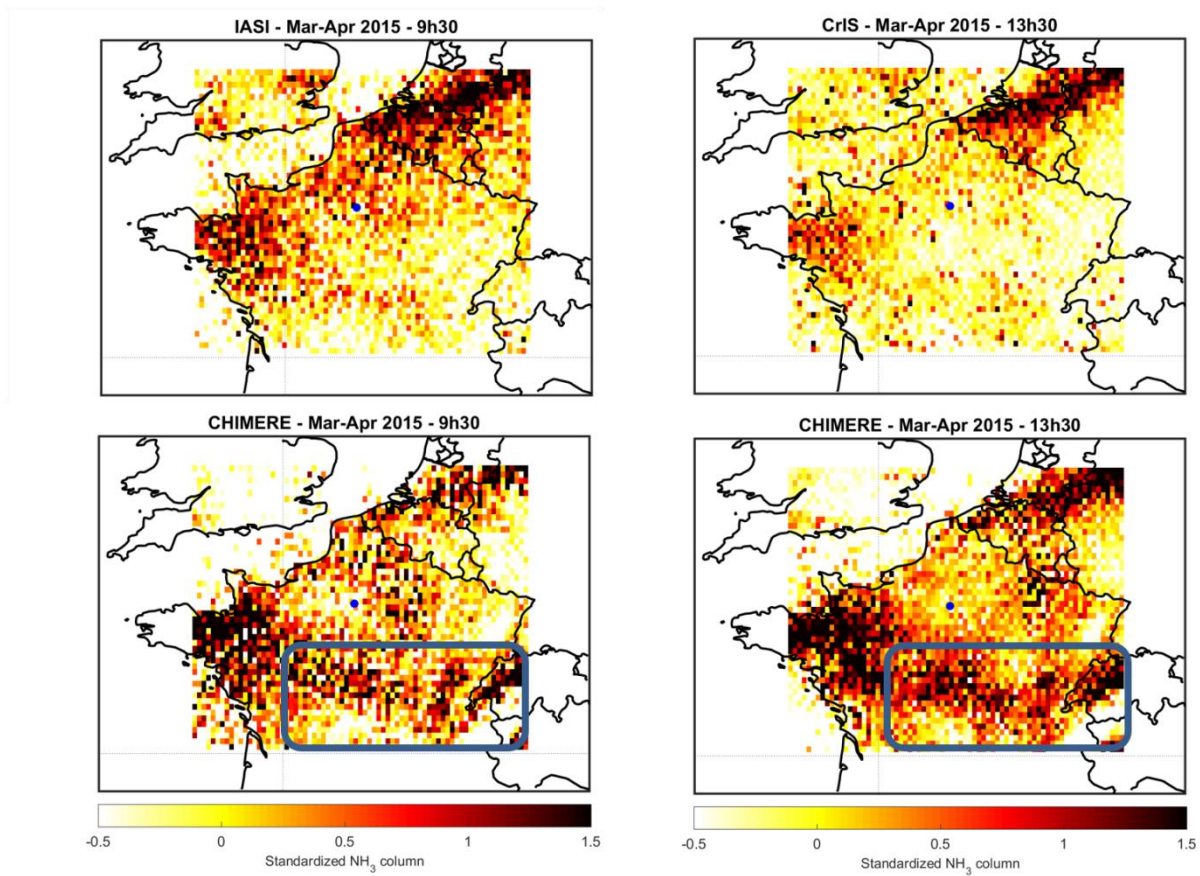
984

985 Figure 7: Correlation plots between monthly means NH_3 standardized concentrations derived
 986 from satellite observations (IASI in red and CrIS in black) and the CHIMERE outputs for the
 987 March to August months of 2014 and 2015. The 1:1 line is represented in the dashed line. Error
 988 bars represent the one-sigma standard deviation around the monthly means.



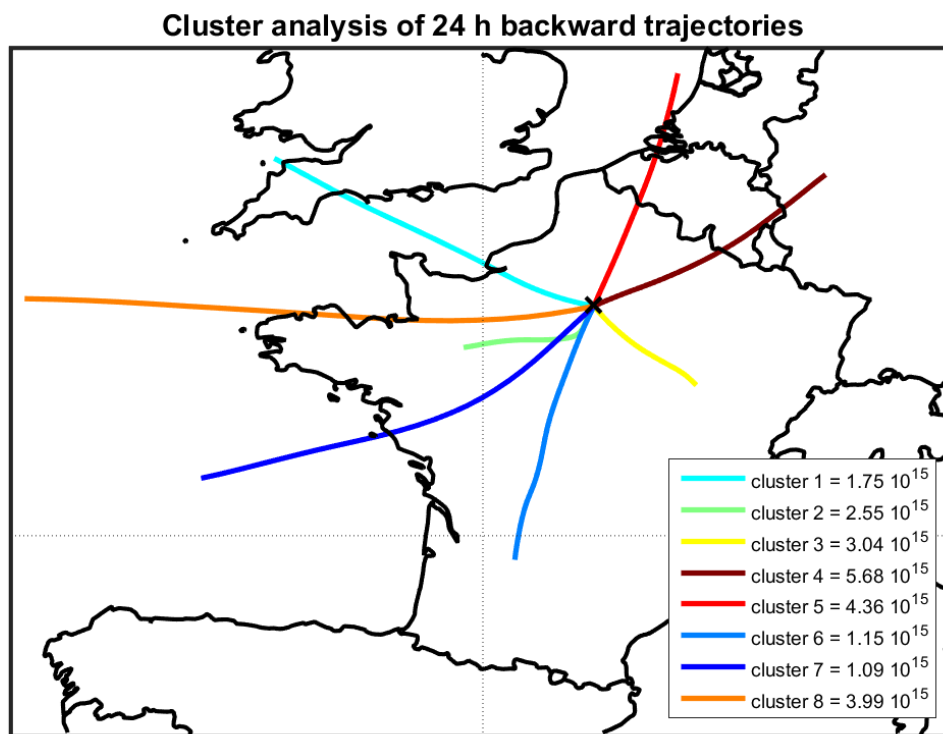
989

990 Figure 8: Standardized NH_3 column derived from the satellite instruments (IASI = top left panel,
 991 and CrIS = top right panel) and the corresponding NH_3 column derived from the CHIMERE model
 992 (coincident with IASI – bottom left panel, and coincident with CrIS – bottom left panel) for
 993 March-April 2014. Blue dots indicate Paris location.



994

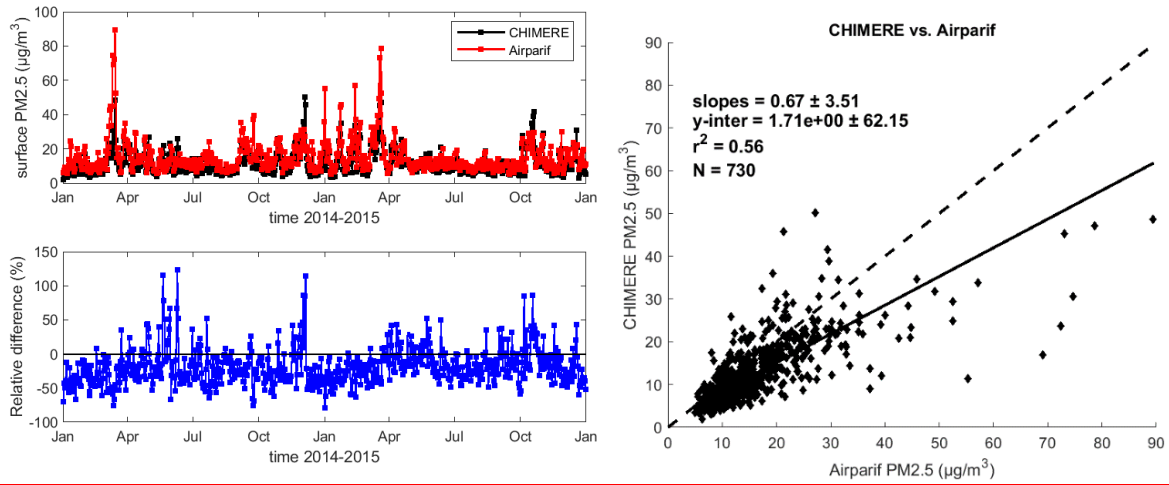
995 | Figure 9: Same ~~asthan~~ Figure 7 but for March-April 2015.



996
 997 Figure 10: Cluster analysis of 24-h backward trajectories arriving in spring in Paris (from
 998 February 15th to May 15th for the 2013-2016 period) using HYSPLIT-4 model obtained from the
 999 NOAA Air Resources Laboratory. Mean trajectories of the 8 clusters are shown in different
 1000 colors, associated with the NH₃ concentrations measured by IASI in the IdF region (in
 1001 molecules/cm⁻²).

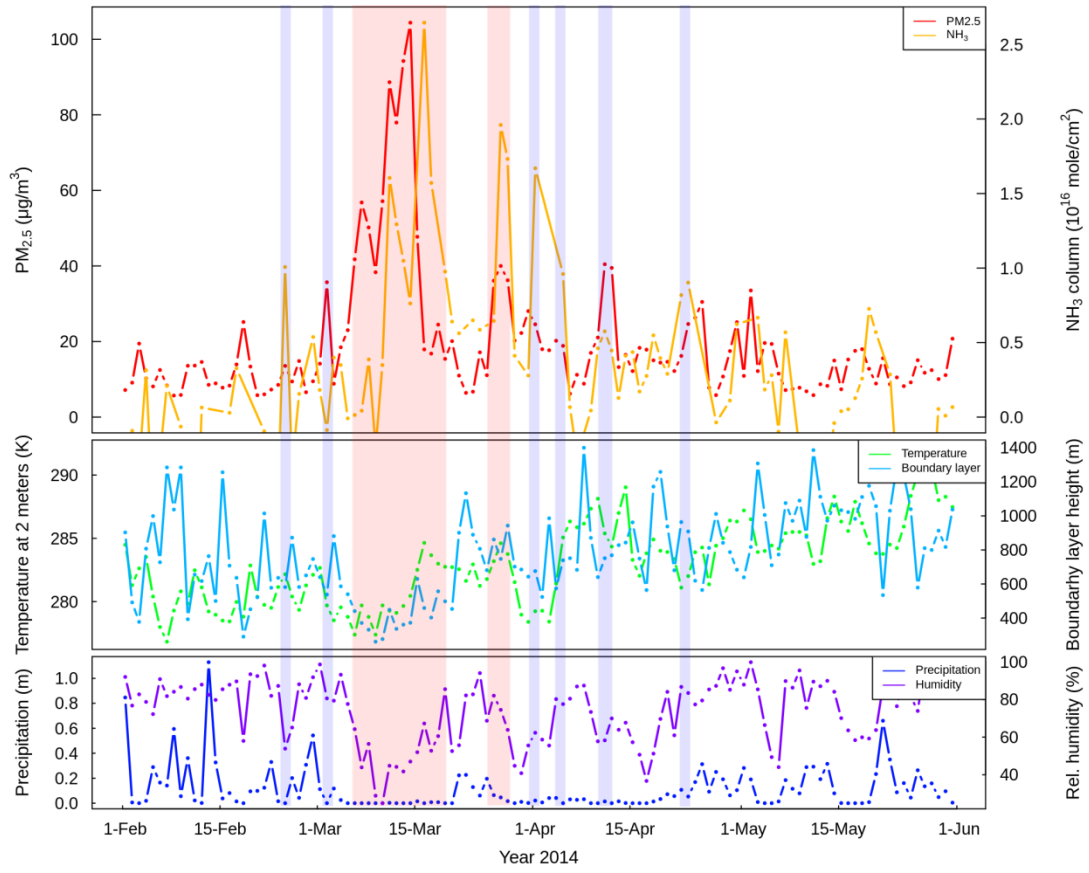
1002

1003

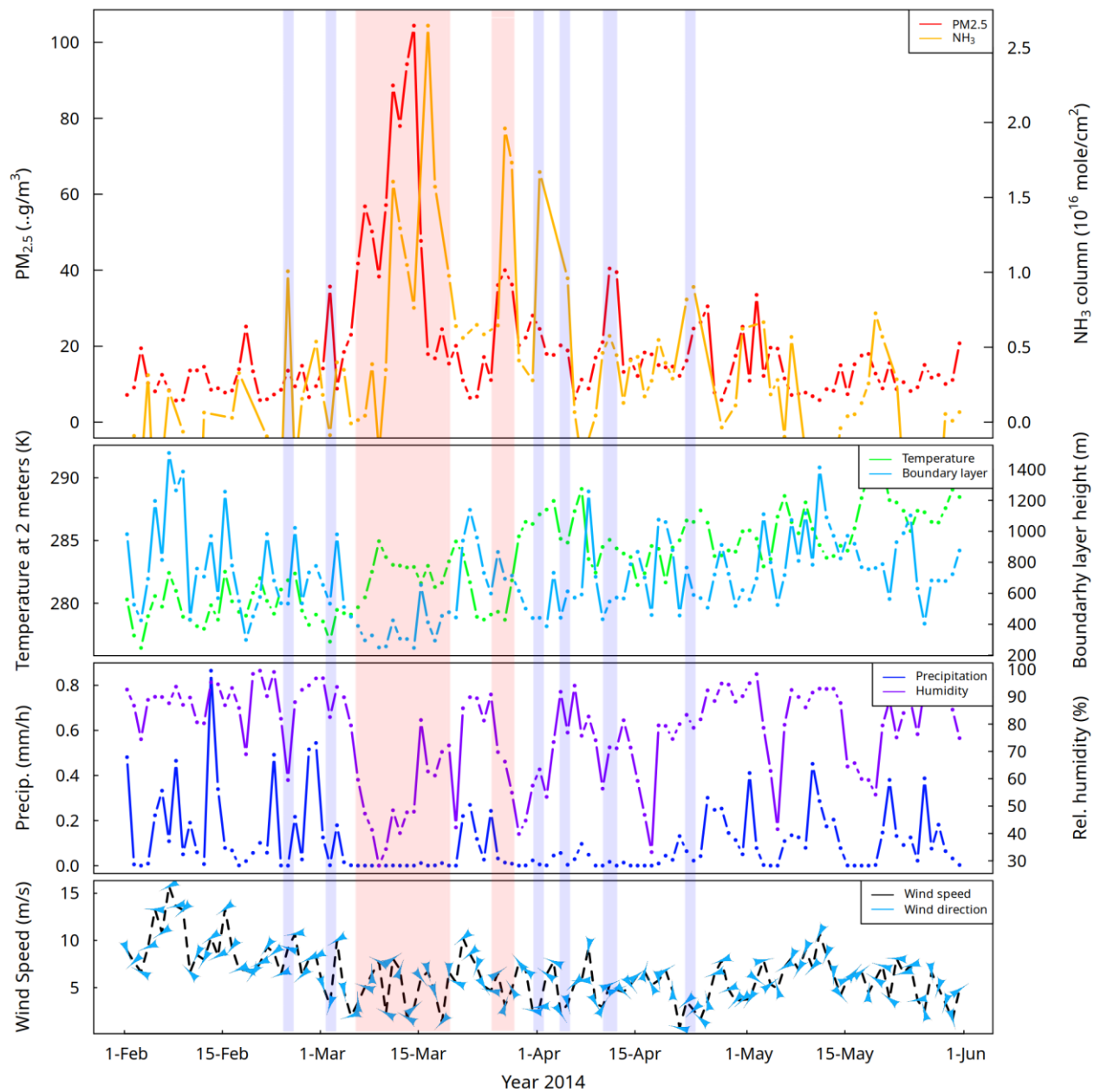


1004

1005 Figure 11: Comparison between PM_{2.5} concentrations derived from the Airparif network and the
1006 CHIMERE model outputs. Left panel: time serie of the daily mean PM_{2.5} concentrations (in
1007 µg/m³) observed at the surface with the Airparif network (red) and calculated with the CHIMERE
1008 model (black), associated with relative differences (in %) calculated as model-observations for
1009 2014 and 2015. Right panel: correlation plots between daily mean PM_{2.5} concentrations derived
1010 from the CHIMERE model versus the Airparif network.

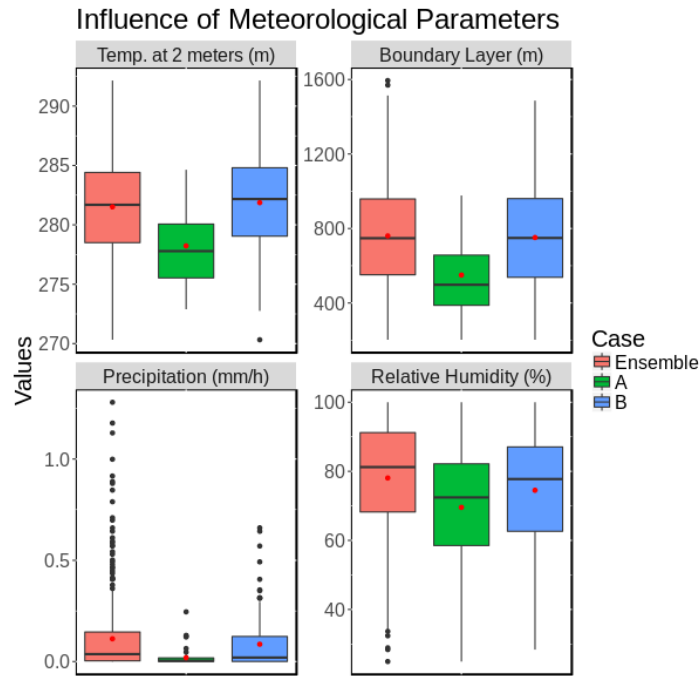


1011

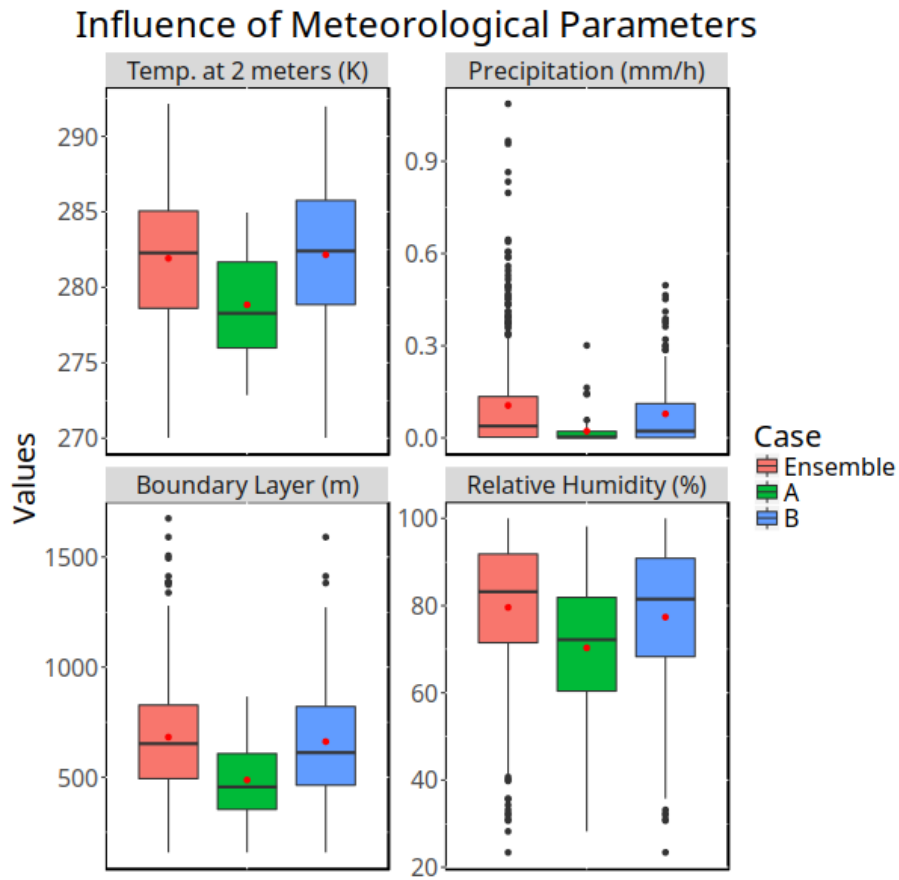


1012
 1013 Figure 124: Average concentrations of NH₃ total columns derived from IASI (in molecules/cm²;
 1014 orange, upper panel) and PM_{2.5} derived from the Airparif network selected within 2 hours from
 1015 the IASI overpass (in µg/m³; red, upper panel) for 2014 as example. Periods of simultaneous
 1016 (independent) enhancements of NH₃ and PM concentrations are represented with red (blue)
 1017 areas, i.e. case A (case B). Temperature at 2 meters (in Kelvin; green, upper middle panel),
 1018 boundary layer height (in meter; blue, upper middle panel), precipitation (in meter; dark blue,
 1019 lower middle panel), and relative humidity (in percent; purple, lower middle panel), and wind
 1020 speed and directions (lower panel) derived from the ECMWF ERA-interim5.

1021



1022



1023 Figure 132: Statistical distributions of meteorological parameters corresponding to case A, case
1024 B, and all observations derived from 2013 to 2016. The medians and the quartiles are presented

1025 by center lines and borders of the boxes, respectively. The mean values are indicated by red
1026 points, and the extreme values (i.e. those beyond $Q1 - 1.5 \text{ IQR}$ and $Q3 + 1.5 \text{ IQR}$) by black points.
1027 The IQR is the "interquartile range", and it equals to $Q3 - Q1$ where $Q3$ and $Q1$ are the 75th and
1028 25th percentiles. Setting the thresholds at $Q1 - 1.5 * \text{IQR}$ and $Q3 + 1.5 * \text{IQR}$ is a common
1029 practice to determine outliers.

1030

TABLE

Satellite	Overpass time (LT)	Time coverage	Nadir spatial resolution (km)	Spectral range (cm ⁻¹)	Spectral resolution (cm ⁻¹)	Spectral Noise* (K) @270K @ 970 cm ⁻¹	References
IASI Metop-A/B	9.30 (AM/PM)	2006-present	12	645–2760	0.5 (apodized)	~0.2	Clerbaux et al., 2009
CrIS Suomi-NPP	1.30 (AM/PM)	2011-present	14	645–1095; 1210–1750; 2155–2550	0.625; (unapodized)	~0.05	Zavyalov et al., 2013

*Spectral noise comparison values in main ammonia spectral region (~970 cm⁻¹) obtained from Zavyalov et al., 2013.

1032 Table 1: Instrumental specifications for the IASI and CrIS satellite instruments.